Article

Cell Host & Microbe

Discovery of ultrapotent broadly neutralizing antibodies from SARS-CoV-2 elite neutralizers

Graphical abstract

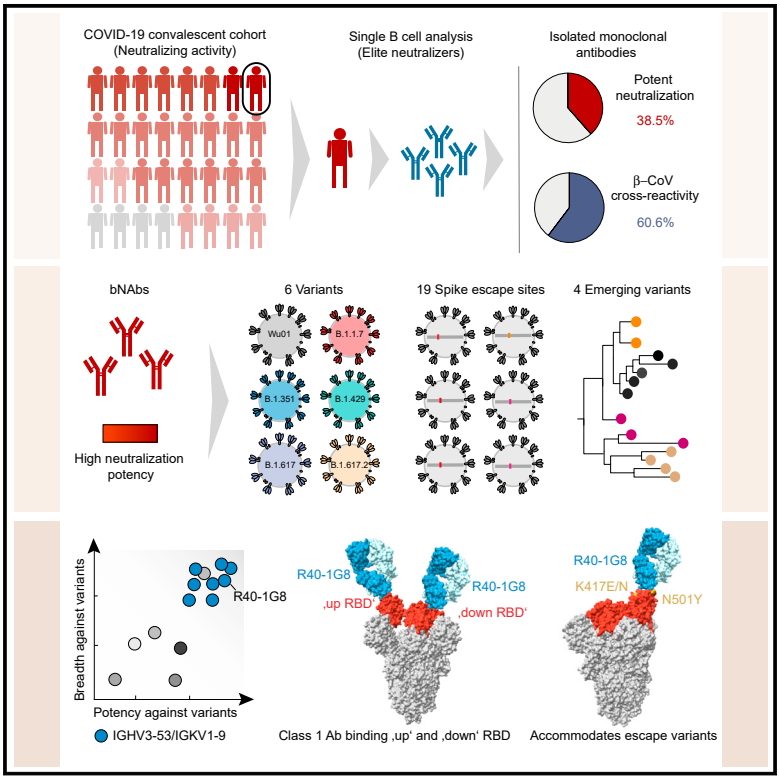

Highlights

- SARS-CoV-2 elite neutralizers are a source for highly potent antibodies
- Isolated bNAbs are highly active against VOCs and emerging variants
- The majority of isolated bNAbs utilized a IGHV3-53/IGKV1-9 gene segment combination
- R40-1G8 is a class-1 RBD bNAb that binds to both “up” and “down” RBD

Authors

Kanika Vanshylla, Chengcheng Fan, Marie Wunsch, ..., Michael Lässig, Pamela J. Bjorkman, Florian Klein

Correspondence

florian.klein@uk-koeln.de

In brief

Vanshylla et al. deciphered the antibody response in SARS-CoV-2 convalescent elite neutralizers on a single B cell level. Isolated antibodies were highly potent and neutralized various mutants, including the predominant variants of concern and emerging variants. Structural analysis of one potent IGHV3-53/IGKV1-9 bNAb revealed a flexible binding mechanism to the RBD.

Vanshylla et al., 2022, Cell Host & Microbe *30*, 69–82
January 12, 2022
https://doi.org/10.1016/j.chom.2021.12.010

CellPress

Cell Host & Microbe

CellPress

Article

Discovery of ultrapotent broadly neutralizing antibodies from SARS-CoV-2 elite neutralizers

Kanika Vanshylla,[1] Chengcheng Fan,[2] Marie Wunsch,[1] Nareshkumar Poopalasingam,[1] Matthijs Meijers,[3] Christoph Kreer,[1] Franziska Kleipass,[1] Denis Ruchnewitz,[3] Meryem S. Ercanoglu,[1] Henning Gruell,[1] Friederike Münn,[4] Kai Pohl,[4] Hanna Janicki,[1] Tobias Nolden,[5] Simone Bartl,[5,6] Saskia C. Stein,[7] Max Augustin,[8] Felix Dewald,[1] Lutz Gieselmann,[1] Philipp Schommers,[8,9] Thomas F. Schulz,[7] Leif Erik Sander,[4] Manuel Koch,[10,11] Marta Łuksza,[12] Michael Lässig,[3] Pamela J. Bjorkman,[2] and Florian Klein[1,9,11,13,*]

[1]Institute of Virology, Faculty of Medicine and University Hospital Cologne, University of Cologne, 50931 Cologne, Germany
[2]Division of Biology and Biological Engineering, California Institute of Technology, Pasadena, CA 91125, USA
[3]Institute for Biological Physics, University of Cologne, 50937 Cologne, Germany
[4]Department of Infectious Diseases and Respiratory Medicine, Charité–Universitätsmedizin Berlin, Freie Universität Berlin and Humboldt-Universität Berlin, 13353 Berlin, Germany
[5]Vira Therapeutics GmbH, 6063 Rum, Austria
[6]Boehringer Ingelheim International GmbH, Ingelheim, Germany
[7]Institute of Virology, Hannover Medical School, Hannover, Germany
[8]Department I of Internal Medicine, Faculty of Medicine and University Hospital Cologne, University of Cologne, 50937 Cologne, Germany
[9]German Center for Infection Research, Partner Site Bonn-Cologne, 50931 Cologne, Germany
[10]Institute for Dental Research and Oral Musculoskeletal Biology and Center for Biochemistry, Faculty of Medicine and University Hospital Cologne, University of Cologne, 50931 Cologne, Germany
[11]Center for Molecular Medicine Cologne (CMMC), University of Cologne, 50931 Cologne, Germany
[12]Department of Genetics and Genomic Sciences, Icahn School of Medicine at Mount Sinai, New York, NY 10029, USA
[13]Lead contact
*Correspondence: florian.klein@uk-koeln.de
https://doi.org/10.1016/j.chom.2021.12.010

SUMMARY

A fraction of COVID-19 convalescent individuals mount a potent antibody response to SARS-CoV-2 with cross-reactivity to SARS-CoV-1. To uncover their humoral response in detail, we performed single B cell analysis from 10 SARS-CoV-2 elite neutralizers. We isolated and analyzed 126 monoclonal antibodies, many of which were sarbecovirus cross-reactive, with some displaying merbecovirus- and embecovirus-reactivity. Several isolated broadly neutralizing antibodies were effective against B.1.1.7, B.1.351, B.1.429, B.1.617, and B.1.617.2 variants and 19 prominent potential escape sites. Furthermore, assembly of 716,806 SARS-CoV-2 sequences predicted emerging escape variants, which were also effectively neutralized. One of these broadly neutralizing potent antibodies, R40-1G8, is a IGHV3-53 RBD-class-1 antibody. Remarkably, cryo-EM analysis revealed that R40-1G8 has a flexible binding mode, targeting both "up" and "down" conformations of the RBD. Given the threat of emerging SARS-CoV-2 variants, we demonstrate that elite neutralizers are a valuable source for isolating ultrapotent antibody candidates to prevent and treat SARS-CoV-2 infection.

INTRODUCTION

The coronavirus disease 2019 (COVID-19) pandemic has led to loss of over 5 million lives worldwide in the last 2 years (Dong et al., 2020). Although a majority of severe acute respiratory syndrome coronavirus 2 (SARS-CoV-2) infections are mild, hospitalizations and death can occur in all age groups, and older individuals with co-morbidities, in particular, are at risk (Williamson et al., 2020). The rapid and successful development of effective SARS-CoV-2 vaccines has been a critical breakthrough (Krammer, 2020). Vaccines can protect from severe disease and death as well as mitigate the spread of infection (Thompson et al., 2021). However, unvaccinated individuals and vulnerable groups such as immune-deficient patients who cannot mount adequate immune responses still remain susceptible to infection and severe complications (Choi et al., 2020). Moreover, the current rise in SARS-CoV-2 variants with antigenic escape mutations can reduce the efficacy of currently approved vaccines and result in increased incidents of breakthrough infections (Lopez Bernal et al., 2021). This warrants the need for interventions which can effectively treat SARS-CoV-2 infection by preventing severe disease and reducing morbidity.

Neutralizing antibodies (NAbs) are an important part of the humoral immune system for preventing viral infections and are crucial for protection (Khoury et al., 2021). They can block viral entry into cells and mediate clearance of viral particles through Fc-mediated effector functions (Zohar and Alter, 2020). Advanced single B cell analyses have helped decipher the B cell response to SARS-CoV-2 and resulted in the isolation of several highly potent monoclonal antibodies (mAbs) (Andreano et al., 2021; Ju et al., 2020; Kreer et al., 2020b; Liu et al., 2020; Robbiani et al., 2020; Rogers et al., 2020; Zost et al., 2020). These SARS-CoV-2 antibodies are directed against the spike (S) protein, which facilitates viral entry into human cells by binding to the human ACE-2 receptor (Hoffmann et al., 2020a; Walls et al., 2020) and is expressed on the virus surface (Piccoli et al., 2020). On the spike protein, a large fraction of the NAb response is directed at the receptor binding domain (RBD) (Piccoli et al., 2020) or the N-terminal domain (NTD) of the SARS-CoV-2 spike S1 domain (Liu et al., 2020). The S2 domain of the spike protein is more conserved than the S1 among β-coronaviruses (β-CoVs) (Cui et al., 2019); however, described NAbs targeting the S2 domain are rare and less potent (Pinto et al., 2021; Sauer et al., 2021). The highly potent neutralizing capacity of RBD-directed antibodies (Dejnirattisai et al., 2021) has led to the clinical development of mAbs for treating and preventing COVID-19 (Corti et al., 2021). Passive immunization with mAbs can prevent infection in exposed individuals (O'Brien et al., 2021) as well as treat COVID-19 and prevent progression to severe disease (Chen et al., 2021b; Dougan et al., 2021; Weinreich et al., 2021). Several of these mAbs have received emergency Food and Drug Administration and European Medicines Agency approval for treatment of COVID-19 or are currently being investigated in phase-III clinical trials (Corti et al., 2021).

Despite the success of antibody-mediated treatment, the recent emergence of SARS-CoV-2 variants with antigenic escape mutations in the spike has led to reduced effectiveness or rendered approved antibodies ineffective due to loss of neutralizing activity (Hoffmann et al., 2021; U.S. Department of Health & Human Services, 2021; Wang et al., 2021). Therefore, it is essential to develop next-generation mAbs that retain potency and effectiveness against circulating or emerging SARS-CoV-2 variants.

We recently studied the NAb response in a SARS-CoV-2 convalescent cohort of 963 individuals (Vanshylla et al., 2021). The NAb response was found to be highly diverse with some individuals lacking any detectable NAb response following natural infection, while others demonstrated a highly potent NAb response. The latter group of so-called ''elite neutralizers'' not only displayed high potency against SARS-CoV-2 but also had cross-reactive antibodies against SARS-CoV-1. In order to understand the Ab response in these individuals, we isolated 1,361 single B cells and produced mAbs from 10 donors. Based on a detailed B cell repertoire analysis, functional antibody characterization and cryoelectron microscopy (cryo-EM) structure determination, we identified diverse β-CoV cross-reactive antibodies as well as a large pool of SARS-CoV-2 broadly neutralizing antibodies (bNAbs). These bNAbs are ultrapotent against circulating SARS-CoV-2 variants of concern (VOCs) as well as emerging escape variants derived from phylogenetic tracking of global SARS-CoV-2 sequences. Therefore, these bNAbs isolated from elite neutralizers serve as an important resource to combat emerging SARS-CoV-2 variants as well as potential future CoV pandemics.

RESULTS

Identification of SARS-CoV-2 elite neutralizers

We recently analyzed the NAb response in a cohort of SARS-CoV-2 convalescent individuals (n = 963) (Figure 1A) (Vanshylla et al., 2021). The neutralizing capacity of the cohort was measured by testing purified plasma immunoglobin G (IgG) in a Wu01-spike-based SARS-CoV-2 pseudovirus assay. The analysis revealed a small fraction of the cohort (3.3%) displaying a highly potent neutralizing response with IgG 50% inhibitory concentration (IC_{50}) values of <20 μg/mL (Figure 1A) and were identified as elite neutralizers (Vanshylla et al., 2021). Ten of these individuals (R040, R121, R200, R207, R259, R339, R410, R568, R616, and R849), ranging in age from 32 to 60 years old (median age: 52), served as donors for single B cell evaluation (Table S1A).

The potency of the IgG response against SARS-CoV-2 in selected subjects ranged from 0.7 to 31 μg/mL (geometric mean IC_{50}: 8.6 μg/mL) (Figure 1B; Table S1B). Moreover, all these individuals also had a highly potent IgG response against SARS-CoV-1 with IgG IC_{50} ranging between 5.1 and 391.7 μg/mL (geometric mean IC_{50}: 36.3 μg/mL) (Figure 1B; Table S1B). Examination of the IgG binding to the SARS-CoV-2 RBD, NTD, and S1 and S2 domains, as well as soluble full-length trimer, revealed reactivity against all regions of the spike (Figure S1A; Table S1B). Moreover, elite-neutralizer-derived IgG demonstrated broad β-CoV reactivity against spike proteins of sarbecovirus (SARS-1) and merbecovirus (MERS) as well as the common cold embecoviruses (OC43 and HKU-1) (Figure S1A; Table S1B). The elite neutralizers also displayed neutralizing IgA antibodies with IC_{50}s ranging from 3.0 to 110.5 μg/mL but with overall lower potency compared to IgG against the SARS-CoV-2 spike (Figures S1B and S1C; Table S1B). In addition to antibody responses, we also tested T cell reactivity against the SARS-CoV-2 spike protein using peptide pools spanning either the S1 or S2 domain (Figures S1D–S1F). PBMC samples from elite neutralizers were compared to high, average, or low neutralizers from the same convalescent cohort (Table S1C) (Vanshylla et al., 2021). We found higher levels of activation-induced marker positive (AIM+) CD4 T cells in elite neutralizers (geometric mean frequency: 0.06%) as compared to high (geometric mean frequency: 0.02%), average (geometric mean frequency: 0.008%), or low neutralizers (geometric mean frequency: 0.008%); however, these differences did not reach statistical significance (Figure S1F). This is in line with previous reports on partial correlation between B and T cell responses to SARS-CoV-2 spike in convalescent individuals (Figure S1F) (Rydyznski Moderbacher et al., 2020). Together, these results demonstrate that elite neutralizers generate a highly potent NAb response against SARS-2 and possess pan-β-CoV reactivity after natural SARS-CoV-2 infection. Thus, such individuals may serve as an ideal source for the identification of novel broad and ultrapotent SARS-CoV-2 mAbs (Figure 1C).

Convergent evolution of B cell response in elite neutralizers

To decipher the B cell response on a single-cell level, we used a pre-fusion stabilized HexaPro SARS-CoV-2 spike protein

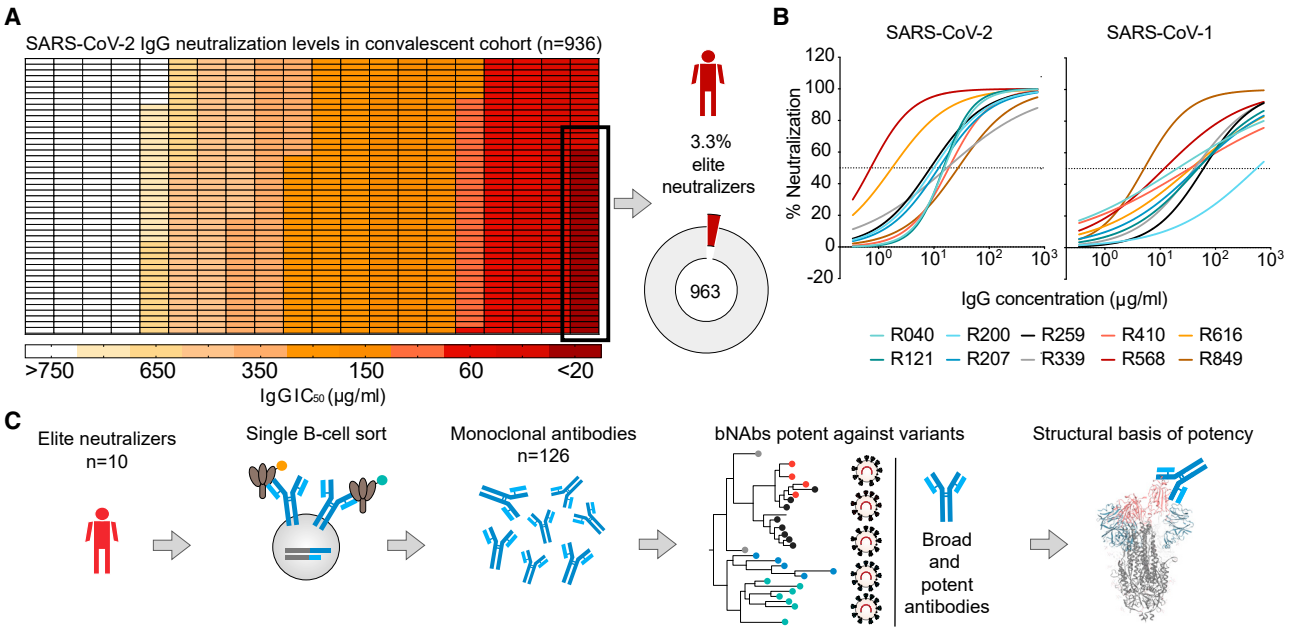

Figure 1. Identification of SARS-CoV-2 elite neutralizers

(A) Heatmap depicting the IgG neutralization IC_{50} values against the SARS-CoV-2 Wu01 pseudovirus in the COVID-19 convalescent cohort studied (Vanshylla et al., 2021). Pie chart shows the fraction of elite neutralizers in the cohort (3.3%).

(B) Neutralization curves depicting IgG neutralization from n = 10 donor elite neutralizers against SARS-CoV-2 and SARS-CoV-1 pseudovirus. Mean of two measurements plotted and dotted line represents 50% neutralization.

(C) Schematic of study design used to identify and isolate monoclonal antibodies from SARS-CoV-2 elite neutralizers.

(Hsieh et al., 2020) as bait to sort antigen-specific B cells from all 10 individuals. The frequency of spike-reactive B cells that bound to both Dylight488-labeled and Dylight650-labeled spike protein bait ranged from 0.4% to 2.1% of the enriched IgG+ B cell fraction (Figure S2A). Reverse transcription and PCR amplification from single-sorted B cells yielded a total of 1,361 productive IgG-heavy chain sequences with between 75–162 IgG-heavy chain sequences obtained from each donor (Figure 2A). Within each individual, 10%–33% of the isolated sequences were clonal with a median B cell-clone size of two, indicating a low clonal expansion and a diverse polyclonal response (Figure 2B). Similar to other COVID-19 convalescent individuals (Cerutti et al., 2021; Chen et al., 2021a; Yuan et al., 2020), the SARS-CoV-2 spike-specific antibodies from elite neutralizers had a relative enrichment for IGHV3-30 (12.8%), IGHV1-69 (10.4%), IGHV4-59 (5.5%), IGHV3-30-3 (5.2%), IGHV1-2 (3.2%), and IGHV3-53 (1.9%) (Figure 2C). A median CDRH3 length of 14 amino acids (aa) (range 5–30 aa) (Figure 2C) and an inferred germline identity of 94% (range 87.4%–100%) was observed (Figure 2C).

COVID-19 convalescent individuals have been shown to produce a shared public B cell clonotype response (Chen et al., 2021a; Nielsen et al., 2020). In order to study whether individuals who show elite neutralization generate similar antibodies, we performed a sequence similarity analysis of all heavy chain sequences. B cell sequences with the same immunoglobin heavy chain variable (IGHV) gene segments were allocated the same cluster if they shared ≥75% CDRH3 similarity (Figure 2D). IGHV3-30, IGHV3-30-3, IGHV3-53, and IGHV4-59 formed among the largest clusters encompassing up to 7 individuals within a cluster with 14 shared sequences (Figure 2D). One IGHV3-30-3 and one IGHV3-53 cluster comprised 26 shared B cell sequences derived from 5 and 3 individuals, respectively. Based on Levenshtein distance calculation, the median CDRH3 distance within clusters ranged from 1–4 amino acids and 6 clusters contained B cells with 2–6 identical CDRH3 sequences (Figure 2D). In summary, SARS-CoV-2 elite neutralizers mount a polyclonal antibody response with a high degree of IGHV sequence similarity, indicating convergent evolution of the antibody response.

SARS-CoV-2 elite neutralizers are a rich source of cross-reactive and ultrapotent antibodies

In order to functionally analyze the SARS-CoV-2 antibody response of elite neutralizers, we cloned and produced 126 mAbs, representing different heavy and light chain gene segment combinations including IgHV3-30 (16.6%), IgHV1-69 (9.5%), IgHV3-30-3 (7.9%), IgHV3-53 (11.1%), IgKV3-20 (19%), IgKV1-9 (11.9%), and IgLV1-40 (6.3%) (Figure S2B). All antibodies were tested in ELISA for reactivity against the SARS-CoV-2 trimer, RBD, and S1 and S2 domains, as well as SARS-1, MERS, HKU-1, and OC43 spike proteins (Figure 3A). Neutralizing activity against SARS-CoV-2 was determined by using a spike-based pseudovirus assay (Figure 3A) as well as authentic virus assay (Figure S2C). In addition, neutralizing activity against SARS-CoV-1 and the bat CoV WiV1, which share the same receptor and have high sequence similarity with SARS-CoV-2 (Hoffmann et al., 2020a), was tested in pseudovirus assays (Figure 3A).

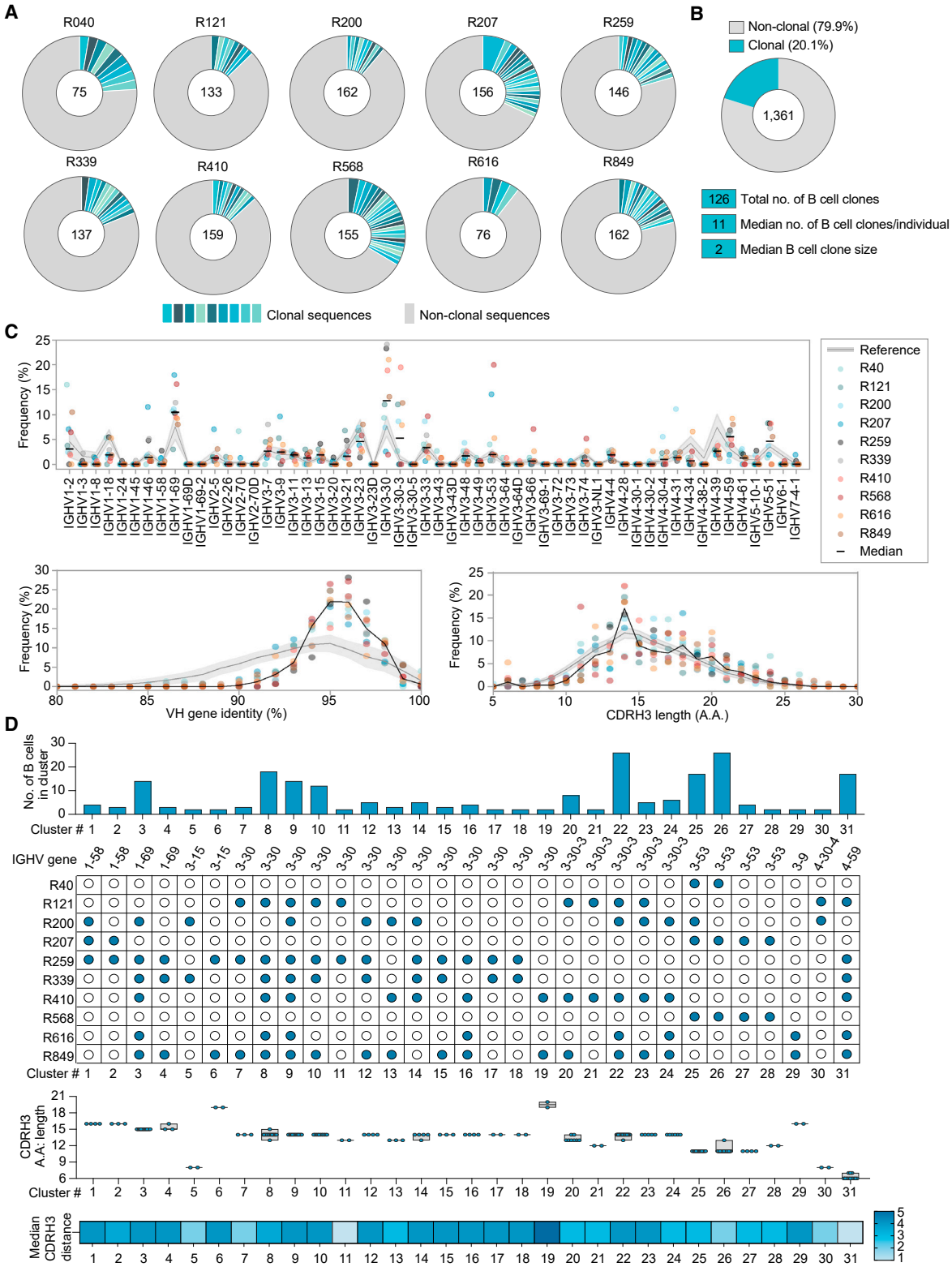

Figure 2. Single B cell analysis of the antibody response against SARS-CoV-2 in elite neutralizers

(A) Pie charts depicting distribution of clonal (shades of blue) and non-clonal (gray) single B cell-derived heavy chain sequences from each elite neutralizer. (B) Pie chart illustrating overall clonality of all productive (n = 1,361) SARS-CoV-2 reactive heavy chain B cell sequences. Total numbers of sequences analyzed shown in center of pie charts in (A) and (B).

(legend continued on next page)

The majority of mAbs (42.8%) were directed against the RBD, while 38.9% bound to the S2 region and 12.7% of mAbs bound the S1 outside the RBD; only 4 out of 126 antibodies did not bind to the SARS-CoV-2 spike by ELISA (Figures 3A and 3B). Neutralizing activity was detected in 98.1% of RBD-targeting antibodies, 18.8% of non-RBD S1-directed mAbs and only in 2% of S2-binding antibodies (Figure 3C). In line with higher conservation of the S2 domain among β-CoVs (Cui et al., 2019), 41 of 47 cross-reactive mAbs (87.2%) bound to S2 and only 6 mAbs (12.8%) bound to the RBD. Therefore, most RBD-directed antibodies were SARS-CoV-2-specific neutralizers, whereas most non-neutralizing S2 antibodies displayed broader reactivity against other β-CoVs (Figure 3D). Derived from 9 of 10 donors, 39.3% of the mAbs displayed cross-reactivity to SARS-CoV-1 (Figure 3E). Three cross-reactive mAbs (R339-3B5, R121-3A3, and R200-4E9) were also reactive to MERS and OC43 spike proteins. The S2 antibody R339-3B5 displayed exceptional cross-reactivity and could also bind HKU-1, making it pan-β-CoV-reactive (Figure 3A). Finally, R339-3B5, along with seven RBD-directed antibodies, could cross-neutralize SARS-CoV-1 and WiV-1, with R121-3G2 showing IC_{50} values as low as 0.004 and 0.006 μg/mL, respectively (Figure 3E). The pan-β-CoV-reactive R339-3B5 had an IC_{50} of 0.921 μg/mL against SARS-CoV-2; hence, the β-CoV cross-reactive neutralizers were relatively less potent in their neutralizing activity.

Out of the isolated antibody pool, 57 antibodies (47.7%) could neutralize the pseudovirus expressing the Wu01 spike protein, and the vast majority of these—45 antibodies (32.8%)—were ultrapotent with IC_{50} values less than 0.02 μg/mL (20 ng/mL) (Figure 3F). To screen for any auto-reactive properties of selected mAbs, we performed HEp-2 cell assays that determine reactivity against nuclear and cytoplasmic antigens and found no or only minimal binding (Figure S3A). Taken together, elite neutralizers possess a large pool of highly potent RBD-directed NAbs. Additionally, elite neutralizers also possess a fraction of less potent NAbs targeting the RBD or S2 domains that are capable of cross-neutralizing β-Coronaviruses.

NAbs from SARS-CoV-2 elite neutralizers are highly effective against variants of concern

SARS-CoV-2 VoCs/variants of interest (VoIs) with higher transmission rates (Volz et al., 2021) and/or antigenic escape mutations (Harvey et al., 2021) have spread globally in recent months. These VoCs can not only reduce the neutralization capacity of serum from convalescent or vaccinated individuals but have also rendered some clinically tested or approved mAbs less effective (Hillus et al., 2021; Planas et al., 2021; Wang et al., 2021). With the aim to identify the next generation of SARS-CoV-2 bNAbs from elite neutralizers, we tested all 57 NAbs against 5 VoC/VoIs and their ancestor—namely, B.1, B.1.1.7, B.1.351, B.1.429, B.1.617, and B.1.617.2 (Figure S3B)—1 NTD escape mutant, and 17 known RBD escape mutants (Figure 4A). Based on this neutralization map, 23 NAbs had 100% coverage by neutralizing all 24 variants with the most potent antibody, R200-1B9, having an average IC_{50} of 0.001 μg/mL (Figure 4A). In contrast, 3 out of 4 clinically tested mAbs, including DZIF-10c (Halwe et al., 2021; Kreer et al., 2020b), REGN10933 (casirivimab), and REGN10987 (imdevimab) (Hansen et al., 2020) covered only 83%, 78%, and 87% of tested variants, respectively. Only S309 (VIR7831) (Pinto et al., 2020) displayed 100% breadth across all variants tested but with lower potency (average IC_{50}: 0.09 μg/mL) (Figure 4A). Evaluation of the somatic hypermutation rate and the CDR3 length of heavy and light chain sequences indicated slightly higher levels of somatic hypermutations and shorter CDRH3s for the bNAbs (Figure S3C). Of note, 20 out of 23 bNAbs bound to the RBD, two were non-RBD-S1, and one was an S2-binding antibody. Interestingly, we observed that among the 23 bNAbs with 100% breadth, 8 antibodies (35%) utilized the IGHV3-53/IGKV1-9 gene segment combination (Figure 4B; Table S2). When closely comparing bNAbs with 100% breadth against VoCs, 11 RBD-directed bNAbs retained very high potency in contrast to clinical antibodies like the REGN antibodies or DZIF-10c that showed loss of activity against B.1.351 or B.1.429, B.1.617, and a prominent variant, B.1.617.2 (Figure 4C).

In summary, our evaluation of the isolated NAbs from elite neutralizers revealed a large pool of highly potent SARS-CoV-2 bNAbs that exhibit full coverage against the most prevalent VoCs as well as RBD escape sites with retention of potent neutralizing activity.

Next-generation ultrapotent bNAbs against emerging SARS-CoV-2 variants

With constant evolution of the SARS-CoV-2 spike, new sites of possible antigenic escape are continually emerging (Harvey et al., 2021; Hodcroft et al., 2021). From GISAID sequencing data from July 21, 2021, over 716,806 unique quality-controlled sequences were used to construct a full, timed phylogenetic tree of circulating SARS-CoV-2 variants with a computational pipeline utilizing software as described in the methods section (Figures 5A and 5B). This was used to obtain frequencies for the VoCs and RBD mutants (Figures 5A and 5B) as well as frequency trajectories from October 2020 onward (Figure S4A). Global frequencies were also compared to frequencies in regions with high (>60%) or low (<30%) vaccination rates (Figure S4A). Here, no substantial differences in trajectories were observed except for the B.1.1.7 VoC and its corresponding mutations, showing higher distributions in countries with high vaccination, which likely reflects the high prevalence of this VoC in the UK (Figure S4A). Using the phylogenetic tree and trajectory profiles, we could track which spike mutations were circulating in the past, which ones are currently circulating, and which new spike mutations show an increase in frequency (Figure S4A). Using global data, four RBD mutants were identified as potential candidates as emerging spike escape sites: R346S, Q414H, N440K, and T478K (Figures 5B and S4A). Among these sites,

(C) Frequencies of heavy chain V-gene distribution from SARS-CoV-2 elite neutralizers (upper panel) and analysis of heavy chain germline identity and CDRH3 length (lower panels) of IGHV sequences derived from elite neutralizers.
(D) Analysis of rates of sequence similarity in the heavy chain CDRH3 from the SARS-CoV-2 antibody repertoire of elite neutralizers. Top to bottom: analysis of size (number) of B cell clusters, V-gene information and individuals included in the cluster, length of the CDRH3s (bars show min. to max. with line at median), and the median CDRH3 distance. Reference in panels (C) and (D) (gray) refers to IGHV sequences derived from naive donors.

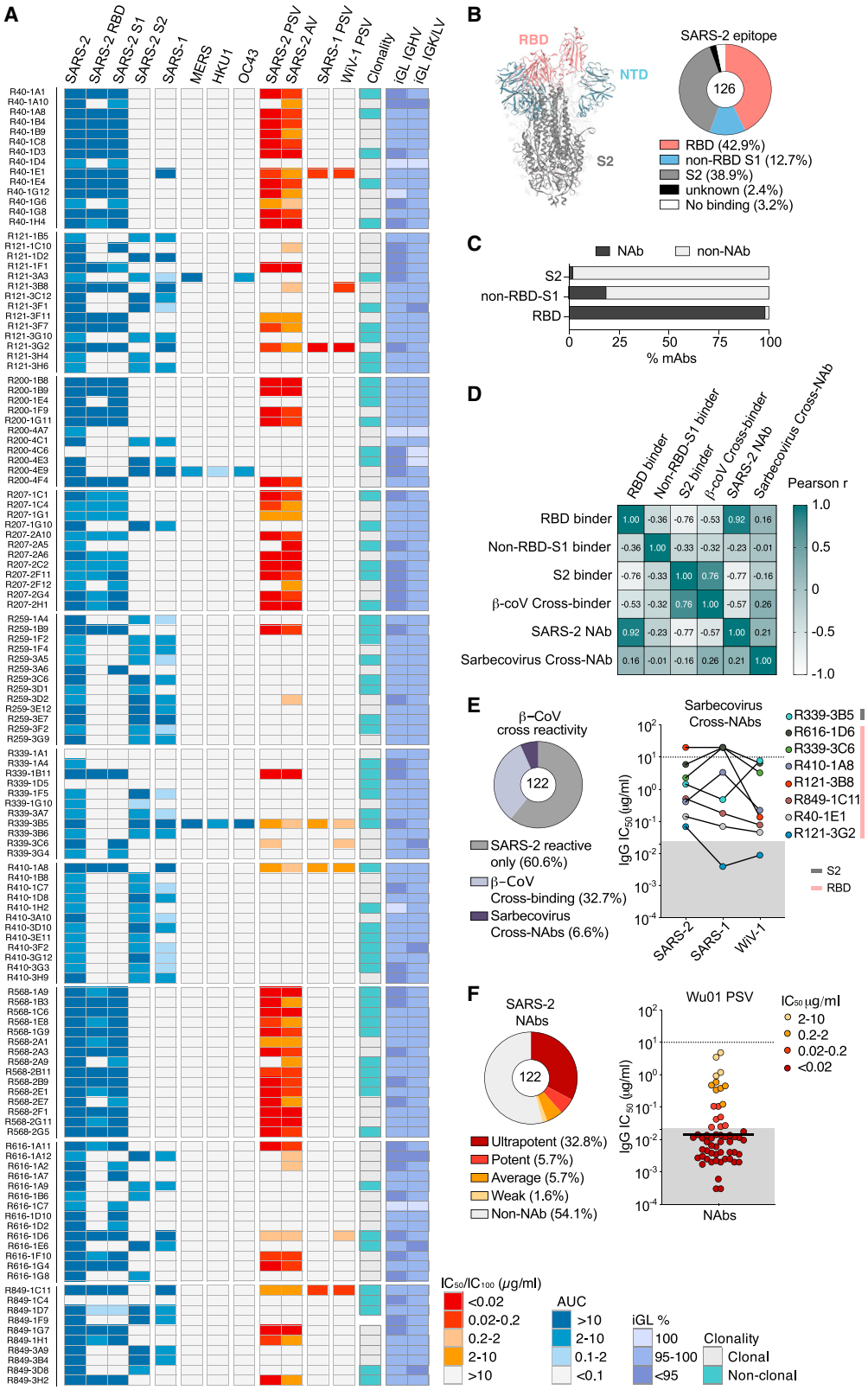

Figure 3. CoV-cross-reactive and potent monoclonal antibodies derived from elite neutralizers

(A) Heatmap illustrating ELISA binding (AUC) against indicated CoV-spikes, pseudovirus neutralization (IC_{50}) (SARS-2, SARS-1, and WIV-1 PSV column), authentic virus neutralization (IC_{100}) (SARS-2 AV column), and clonality and germline identity of n = 126 elite neutralizer mAbs. iGL, inferred germline.

(legend continued on next page)

the T478K mutation is a defining mutation in the B.1.617.2 (delta) VoC spike, R346S in the VoI C.36.3, or R346K in the VoI B.1.621 (mu); Q414H appeared multiple times in the B.1.617.2 clade; and N440K was spread across the phylogenetic tree on multiple backgrounds. We generated pseudovirus variants expressing these mutations in the B.1 (D614G) background and tested all NAbs against them (Figures 5B and S4B). A large fraction of NAbs isolated from elite neutralizers had exceptionally high potency against all 24 variants tested (Figures 4 and S4B). Notably, all 11 RBD ultrapotent bNAbs with exceptional breadth and potency (Figure 4) remained effective against all predicted emerging mutations (Figure 5C). In contrast, the clinical NAbs like DZIF-10c and REGN10987 were affected by mutations at R346 and N440, respectively (Figure 5C).

In summary, bNAbs from elite neutralizers are not only highly potent against the prevalent circulating VoCs but are also effective against emerging escape sites in the spike RBD, thereby constituting next-generation SARS-CoV-2 NAbs that may retain activity despite further virus evolution in the future.

Cryo-EM complex of R40-1G8 Fab with SARS-CoV-2 spike reveals binding to both "up" and "down" RBD

Notably, antibodies utilizing the IGHV3-53 and IGKV1-9 V gene segments are reported to exhibit exceptional SARS-CoV-2 neutralizing potency (Dejnirattisai et al., 2021). We wanted to obtain insight into the binding pattern of the RBD bNAbs to better understand their ability to their high coverage of variants. RBD antibodies are structurally characterized into 4 epitope classes based on their binding epitope, as well as their ability to bind an "up" or "down" RBD conformation and to block ACE2 binding. IGHV3-53 antibodies are typically class 1 or class 2 antibodies, and mutations at K417 or E484, respectively, can knock out the function of these antibodies (Barnes et al., 2020; Harvey et al., 2021). We tested the RBD bNAbs by competition ELISA against C102 (Robbiani et al., 2020), P2B-2F6 (Ju et al., 2020), S309 (Pinto et al., 2020), and Fab2-36 (Liu et al., 2020) as class 1, 2, 3, and 4 reference antibodies, respectively (Figure S5A). Based on these competition data, potent bNAbs showed a high degree of overlap (>90%) among each other and are closely related to class 1 or class 2, which bind to the RBD in an "up" (class 1) or "up and down" (class 2) orientation.

To pin down the binding mode, we selected one of the most potent and broad bNAbs from the pool with overlapping RBD binding for cryo-EM analysis (Figures 6 and S5). The selected bNAb, R40-1G8, is an IGHV3-53/IGKV1-9 antibody with an IC_{50} of 0.001 μg/mL against the Wu01 spike and an average IC_{50} of 0.004 μg/mL across the variant panel (Figure 4). To define the binding epitope, we determined a single-particle cryo-EM structure of SARS-CoV-2 S HexaPro trimer in complex with R40-1G8 Fab in two conformational states of the RBD (Figures 6A and 6B). R40-1G8 Fab was found to bind to both up (state 1) and down (state 2) RBDs, but due to the relative low resolution for the RBD and Fab in state 2 (Figure S5), we only built the model for state 1 with R40-1G8 Fab bound to all up RBDs. Focused refinement of the region of RBD of SARS-CoV-2 S HexaPro trimer bound R40-1G8 resulted in a 3.5 Å local resolution (Table S3; Figure S5). The interaction between R40-1G8 and the RBD was mainly mediated through the heavy chain contacting 16 residues, while the light chain had 6 sites of contact (Figures 6D and 6E). Structural alignments with complex structures of class 1 (C102 and C105) and class 2 (C002) revealed that R40-1G8 binds to a similar epitope as C102 or C105, suggesting it is a class 1 antibody (Figures 6F and S6).

C102 is a class 1 antibody encoded by IGHV3-53 and binds the RBD only in an "up" conformation (Barnes et al., 2020). R40-1G8 seem to be an exception in the class-1 RBD antibody class as it binds both an "up" and "down" RBD conformation (Figures 5, S5, and S6). In addition, many IGHV3-53 antibodies like C102 with a short CDRH3 are affected by the K417 mutation (Wu et al., 2020; Yuan et al., 2021), but despite the similar binding mode (Figures 6F and S6) and CDRH3 length (Table S2), R40-1G8 is not affected by the K417E/N/T mutation, which is a prominent escape site found in VoCs like B.1.351 (Figures 4 and S6). The K417 site in the C102 structure is almost forming a cation-pi interaction in addition to a hydrogen bonding interaction. However, K417 in the R40-1G8 structure does not have this interaction, which explains lack of escape at this residue (Figure S6). R40-1G8 is also not affected by another key mutation at N501Y, which is present in the VoC B.1.1.7, as the antibody can accommodate Y at RBD position 501 (Figure S6). In summary, by examining structural binding properties of R40-1G8, we found a class 1 RBD antibody binding mechanism which encompasses binding to both "up" and "down" RBD, thereby providing structural insights into the high potency and breadth of this bNAb.

DISCUSSION

SARS-CoV-2 elite neutralizers mount a highly potent NAb response following natural infection, which is accompanied by the presence of cross-reactive antibodies against other closely related β-CoVs (Vanshylla et al., 2021). The Ab response in such individuals has not been studied in detail and could prove to be a critical source of potent NAbs as therapeutics to treat or prevent SARS-CoV-2 infection. In this study, we isolated mAbs from 10 elite neutralizers that were identified from screening 963 COVID-19 convalescent individuals. We discovered several ultrapotent RBD-directed antibodies that potently neutralize prevalent VoCs and a panel of prominent RBD escape mutants, as well as an S2-directed NAb with cross-reactivity spanning the SARS-1, MERS, and embecovirus family. Importantly, the isolated bNAbs are able to neutralize all VoCs as well as emerging variants.

(B) Annotated P0DTC2 (6XKL) model of the SARS-CoV-2 spike (left) and pie chart showing epitope-binding distribution of the mAbs determined by ELISA (right).
(C) Bar graph presenting fraction of neutralizing mAbs (n = 122) binding to SARS-CoV-2 spike epitopes.
(D) Pearson correlation matrix of binding and neutralization data from (A) in order to study relationships between binding epitopes, SARS-2-specific neutralization, β-CoV cross-reactivity (SARS-1, MERS, HKU1, and OC43), and sarbecovirus cross-neutralization (SARS-1 and WiV-1).
(E) Pie chart depicting fraction of cross-reactive mAbs (left) and plot depicting IC_{50} values of sarbecovirus cross-neutralizing mAbs (right).
(F) Pie chart depicting fraction of NAbs, based on potency (left), and plot showing IC_{50}s of NAbs against the SARS-CoV-2 Wu01 pseudovirus (right); black bar denotes geometic mean. Gray area in (E) and (F) highlights values below 0.02 μg/mL.

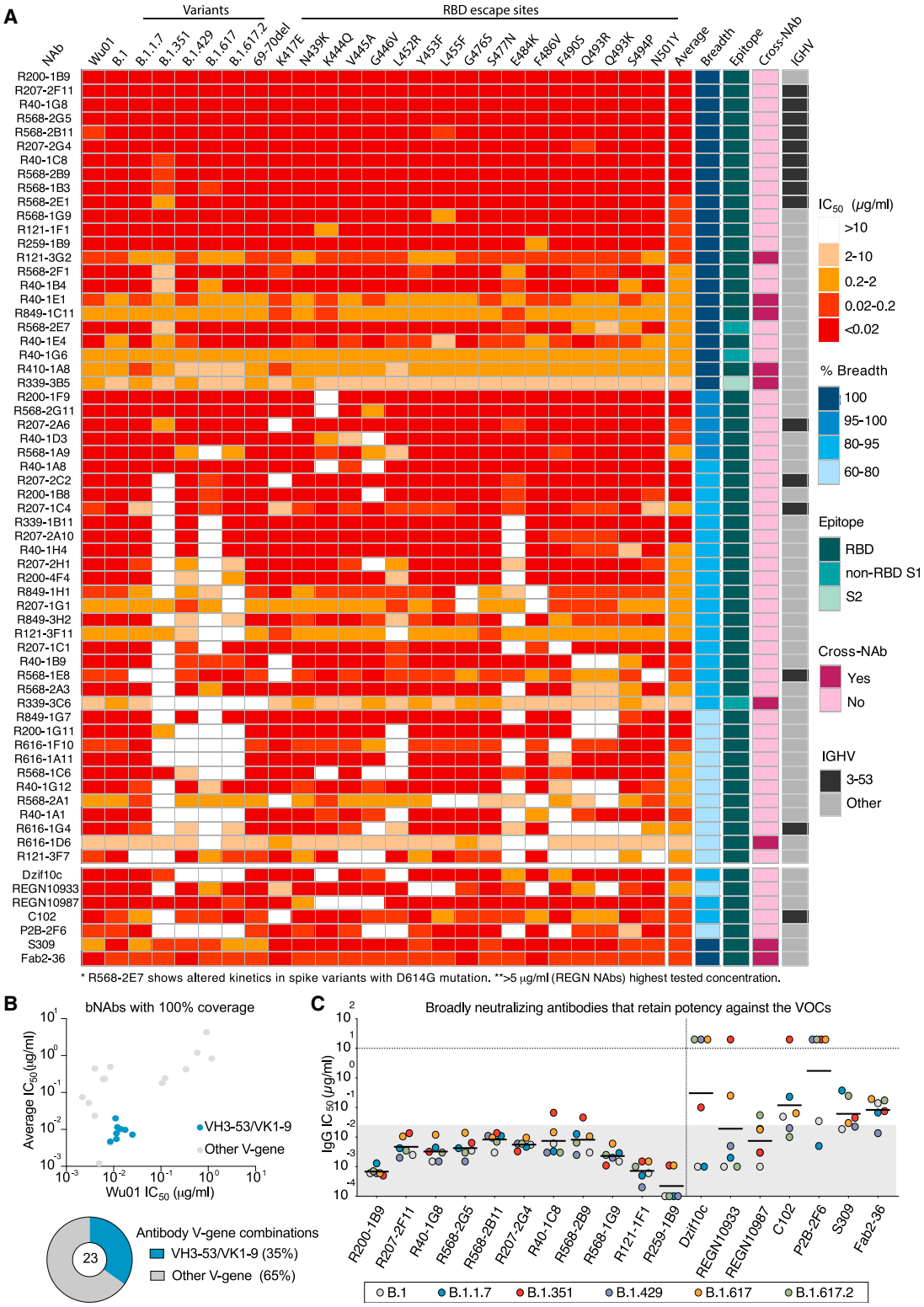

Figure 4. Broadly neutralizing next-generation SARS-CoV-2 bNAbs

(A) Neutralization escape map profile of n = 57 elite neutralizer NAbs against 25 SARS-CoV-2 spike pseudovirus variants. Average IC_{50} values, relative neutralization breadth across the variants, the spike epitope determined by ELISA, and cross-neutralizing capacity, as well as IGHV3-53 usage, are depicted in columns to the right.

(legend continued on next page)

These data confirm that antibody responses of SARS-CoV-2 elite neutralizers are both potent and diverse. Moreover, our analysis resulted in the isolation of NAbs that are ultrapotent against SARS-CoV-2 with 82% of the NAb fraction having IC_{50} values below 0.02 μg/mL. While we do not know why these individuals generate this potent NAb response, the higher anti-spike response in elite neutralizers may help enhance development of cross-reactive antibodies. This is confirmed by β-CoV cross-reactivity in 39% of isolated mAbs, some of which could neutralize SARS-1 with IC_{50}s as low as 0.004 μg/mL. Most cross-reactive mAbs were directed against the S2 domain of the spike protein, which is more conserved among β-CoVs (Pinto et al., 2021; Sauer et al., 2021). However, unlike the RBD, the S2 domain does not induce a high neutralizing response as supported by 89% (41 of 46) of our isolated S2-directed mAbs being non-neutralizing mAbs. The mAb R339-3B5 had neutralizing activity against S2 domain of SARS-CoV-2 with an IC_{50} of 0.9 μg/mL. Although relatively less potent than RBD NAbs, this antibody displayed exceptional cross-reactivity against SARS-1, WiV-1, MERS, HKU1, and OC43, making it one of the few pan-β-CoV reactive antibodies described so far (Pinto et al., 2021). Less potent RBD NAbs were cross-reactive with SARS-CoV-1 and Wiv1 CoVs, and several of these NAbs maintained reactivity against the SARS-CoV-2 variants, suggesting that they target highly conserved sites on the RBD. Cross-neutralizing antibodies targeting the RBD are quite rare (Starr et al., 2021), and S309 (VIR7831), isolated from a SARS-1 survivor, is currently the only cross-reactive RBD antibody in advanced clinical use (Pinto et al., 2020). Targeted introduction of mutations to improve potency of pan-β-CoV-reactive mAbs could make them good candidates for further clinical development.

Although highly efficacious vaccines have been rapidly developed, unvaccinated or immunocompromised patients are in need for effective therapeutics (Choi et al., 2020). SARS-CoV-2 mAbs can reduce the risk of hospitalization (Dougan et al., 2021); however, several clinical SARS-CoV-2 mAb programs have suffered setbacks due to the emergence of SARS-CoV-2 escape variants (Harvey et al., 2021). Thus, the next generation of mAbs need to block circulating and emerging escape variants of SARS-CoV-2. From the elite neutralizers, we isolated NAbs with an average IC_{50} of 0.001 μg/mL against B.1.1.7, B.1.429, B.1.617, B.1.617.2, B.1.351, and 19 single escape sites. Out of the isolated fraction, 23 bNAbs (19%) were identified with 100% coverage across all tested variants. Importantly, potent bNAbs could also cover emerging RBD escape sites at R346S, Q414H, N440K, and T478K. R346 and N440 mutants were previously only reported in cell culture-based escape assays (Liu et al., 2021; Weisblum et al., 2020). The prediction of escape sites by using frequency trajectories and building a phylogenetic tree using 700,000 sequences helps studying variants that are circulating at low levels but might expand in the near future. Therefore, by testing such sites, we predict that the isolated bNAbs are likely to cover variants that may arise in the near future.

Potent antibodies of the IGHV1-24 clonotype targeting the NTD supersite have been described before (Cerutti et al., 2021), but these antibodies are also prone to escape observed within the NTD of VoCs (McCallum et al., 2021). We did not find SARS-CoV-2-specific IGHV1-24 antibodies in the investigated elite neutralizers, but interestingly, many of the highly potent bNAbs targeted the RBD and utilized the IGHV3-53/IGKV1-9 gene segment combination. It was previously shown that antibodies with short CDRH3s are generally class 1 RBD binders and those with long CDRH3s are class 2 RBD binders and are typically knocked out by K417 or E484 mutants respectively (Barnes et al., 2020; Wu et al., 2020; Yuan et al., 2021). Using our set of 5 VoCs and 19 RBD mutants, we identified several IGHV3-53 antibodies that defy this paradigm. Despite being IGHV3-53 antibodies with 93.5%–97.3% germline identity, minor differences in the antibody sequence seem to render them immune from the typical escape seen for this VH class. Cryo-EM structure of one of the IGHV3-53/IGKV1-9 bNAbs, R40-1G8, revealed a unique class 1 antibody mechanism that allows binding of both "up" and "down" conformations. Class 1 antibodies were previously shown to bind an "up" RBD because binding to "down" RBD will have clashes with the nearby RBD. However, in the R40-1G8-spike map, there is one "up" RBD with R40-1G8-Fab, one "up" RBD without R40-1G8-Fab, and a "down" RBD with R40-1G8-Fab. This current state is possible because Fab-free "up" RBD moves out of the way and the "down" RBD can be bound by R40-1G8. This alternative approach to binding the RBD could potentially explain the breadth of R40-1G8 against SARS-CoV-2 variants, as it may provide higher flexibility to this bNAb in approaching the RBD. Such insights will help to guide structure-based vaccine design strategies to effectively counter current and emerging VoCs.

In summary, we demonstrate that SARS-CoV-2 elite neutralizers generate a highly diverse and potent Ab response that can yield β-CoV cross-reactive and SARS-CoV-2 bNAbs with up to 100% coverage against RBD escape variants and VoCs. Together, these findings illustrate that elite neutralizers are excellent candidates for the isolation of next-generation SARS-CoV-2 bNAbs and pan β-CoV antibodies.

STAR★METHODS

Detailed methods are provided in the online version of this paper and include the following:

- KEY RESOURCES TABLE
- RESOURCE AVAILABILITY
  - Lead contact
  - Materials availability
  - Data and code availability
- EXPERIMENTAL MODEL AND SUBJECT DETAILS
  - Enrollment of human subjects and study design
  - Cell lines

(B) Dot plot depicting average IC_{50}s and IC_{50}s against Wu01 for all isolated bNAbs (n = 23) with the IGHV3-53/IGKV1-9 bNAbs highlighted in blue. Pie chart shows fraction of IGHV3-53/IGKV1-9 bNAbs among nBAns obtained from elite neutralizers.
(C) Plot evaluating the IC_{50} values of the broadest (100%) and most potent NAbs against SARS-CoV-2 pseudovirus variants with spike sequence of B.1, B.1.1.7, B.1.351, B.1.429, B.1.617, and B.1.617.2 are compared to published monoclonal antibodies. REGN antibodies tested up to 5 μg/mL. Gray area in (C) highlights values below 0.02 μg/mL, and black bars denote geometric means.

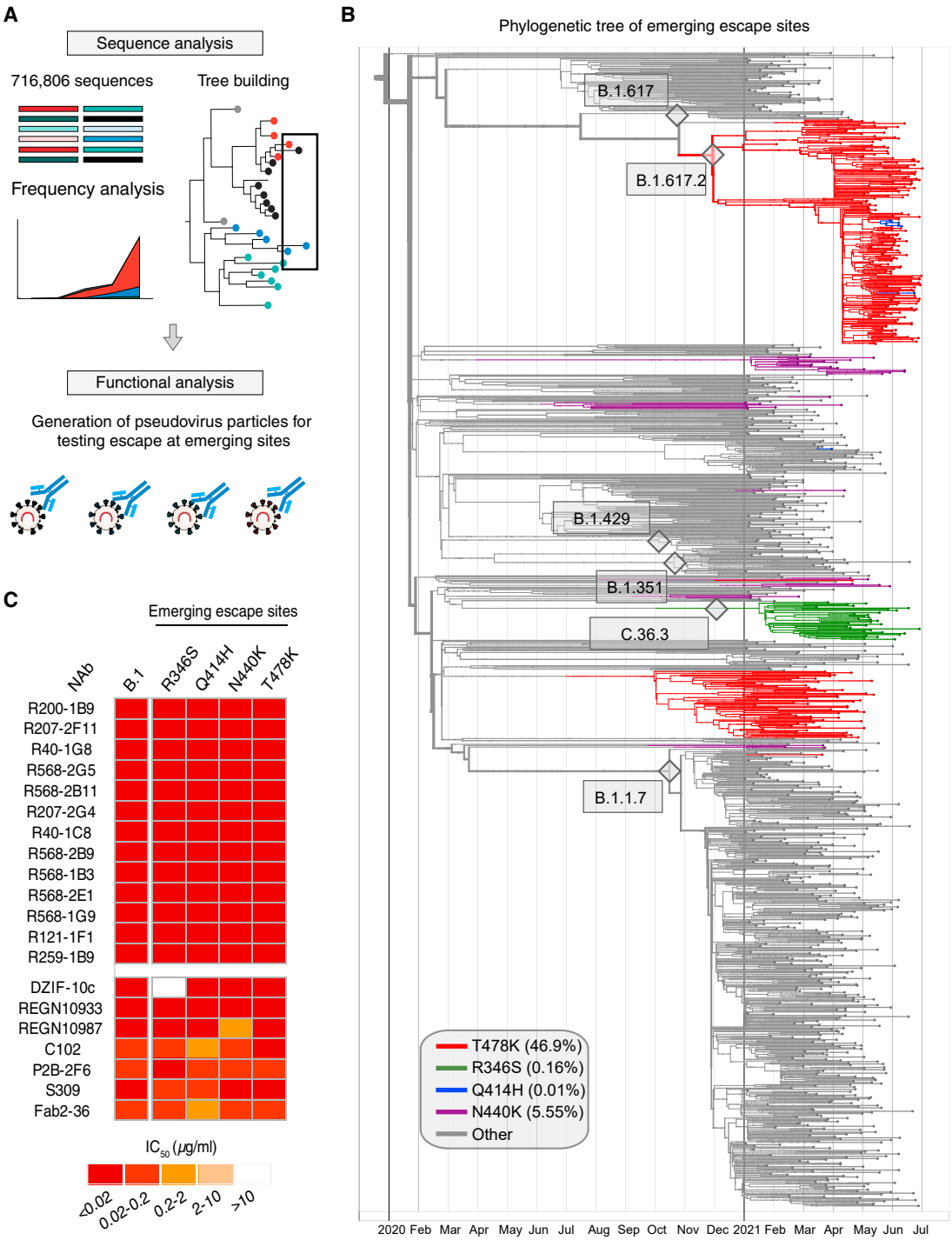

Figure 5. Maintenance of bNAb potency amidst emerging escape variants

(A) Schematic of study design used to analyze emerging escape variants.

(B) A full phylogenetic tree with leaves corresponding to isolated sequences collected after January 01, 2020, highlighting the 4 RBD mutations: T478K (red), R346S (green), Q414H (blue), and N440K (purple). The number of leaves for each clade reflects the frequency of that clade in 2021, where the 4 RBD mutations are upweighted.

(C) Neutralization analysis of the 11 most potent and broad bNAbs along with published antibodies tested against B.1 pseudoviruses carrying the 4 emerging spike mutations, R346S, Q414H, N440K, and T478K.

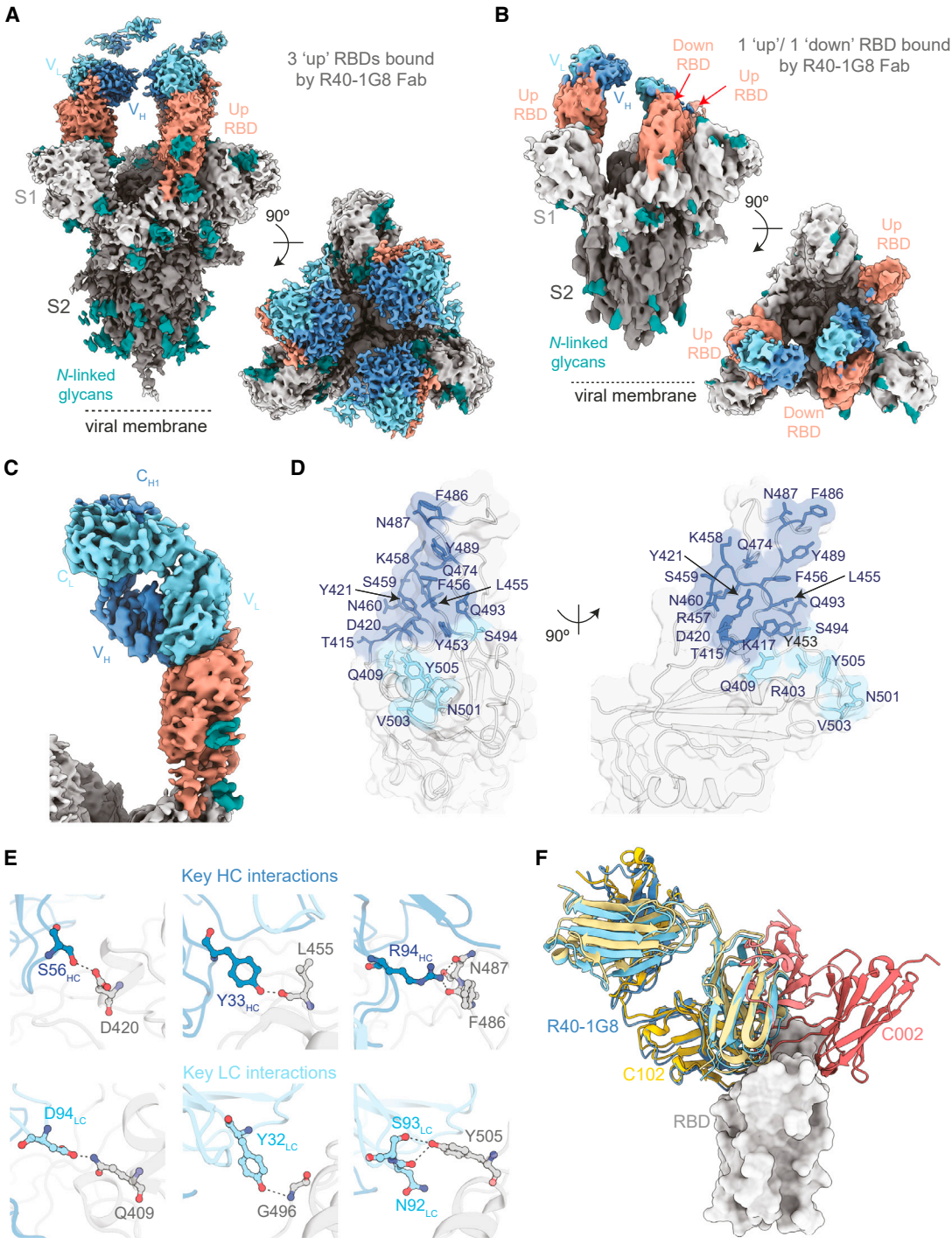

Figure 6. Structural basis of SARS-CoV-2 neutralization breadth of R40-1G8

(A and B) Cryo-EM density maps for R40-1G8 Fab-SARS-CoV-2 S protein complexes at 3.2 Å (state 1) (A) and 3.7 Å (state 2) (B), revealing binding of R40-1G8 Fab to both up and down RBDs as indicated by the orange arrows.

(C) Locally refined cryo-EM map of the R40-1G8 Fab-RBD complex from which the R40-1G8 Fab was built.

(D) Surface representation of the R40-1G8 Fab epitope on the surface of RBD. Epitope residues are shown as sticks in blue (for interactions with the R40-1G8 heavy chain) and light blue (interactions with the R40-1G8 light chain).

(E) Close-up showing interactions between the heavy and light chains of R40-1G8 and RBD with the contact residues involved in key interactions shown in sticks.

(F) Structural alignment of C102 (PDB 7K8M), C002 (PDB 7K8T), and R40-1G8 on the RBD, revealing that R40-1G8 binds at a similar location as the class 1 anti-RBD antibody C102.

- METHOD DETAILS
  - Processing of serum, plasma and whole blood samples
  - Isolation of IgGs and IgAs from serum and plasma samples
  - Single B cell sorting
  - Single cell cDNA production and PCR
  - Antibody sequence analysis
  - Antibody cloning for protein synthesis
  - Antibody synthesis
  - Cloning of SARS-CoV-2 spike variants
  - Production of SARS-CoV pseudovirus particles
  - Pseudovirus assay to determine IgG/plasma/serum neutralizing activity
  - SARS-CoV-2 authentic virus neutralization assay
  - SARS-CoV-2 T cell reactivity assay
  - Production of coronavirus spike proteins
  - Detection of spike-specific reactivity by ELISA
  - Competition ELISA
  - Hep-2 autoreactivity assay
  - Production of Fab fragments and spike protein and sample preparation for cryo-EM
  - Cryo-EM data collection, processing and refinement
- QUANTIFICATION AND STATISTICAL ANALYSIS
  - Statistical modeling of SARS-CoV-2 sequences for identification of variants
  - Statistical analysis

SUPPLEMENTAL INFORMATION

Supplemental information can be found online at https://doi.org/10.1016/j.chom.2021.12.010.

ACKNOWLEDGMENTS

We would like to thank all members of the Klein lab for helpful discussions; Clara Lehmann for critical review of this manuscript and facilitating our work with the COVID-19 outpatient unit; Petra Meyer, Nicole Riet, and Ricarda Stumpf for technical assistance; Daniela Weiland, Nadine Henn, and Susanne Salomon for project and laboratory management; Knut Elbers for support with SARS-CoV-2 spike escape variants; Ching-Lin Hsieh and Jason S. McLellan for the SARS-CoV-2 HexaPro spike construct; Michael Korenkov and the team at Boehringer Ingelheim for antibody plasmids and antibodies; Pauline Hoffman, Dr. Jost Vielmetter, and the Caltech Beckman Institute Protein Expression Center for protein expression and purification; and Dr. Songye Chen for maintaining the electron microscope. Cryo-EM was performed in the Beckman Institute Resource Center for Transmission Electron Microscope at Caltech. This work was funded by grants to M.K. (DFG FOR2722); to P.J.B. by National Institutes of Health (1P01AI138938-S1); to M. Laessig by German Research Foundation (DFG) (CRC1310); to L.E.S. from COVIM "NaFoUniMedCovid19" (FKZ: 01KX2021); to F. Klein from the German Center for Infection Research (DZIF), the DFG (CRC1279 and CRC1310), European Research Council (ERC) (ERC-StG639961), and COVIM "NaFoUniMedCovid19" (FKZ: 01KX2021).

AUTHOR CONTRIBUTIONS

Conceptualization, F. Klein and K.V.; methodology, F. Klein, K.V., M.M., C.K., D.R., and C.F.; formal analysis, K.V., C.F., M.M., C.K., M.W., N.P., F.M., K.P., and H.G.; investigation, K.V., C.F., M.W., N.P., C.K., F. Kleipass, H.J., M.S.E., D.R., H.G., T.N., S.B., M.K., F.M., and K.P.; phylogenetic analysis, M.M.; sequence analysis, C.K.; resources, S.C.S., M.A., F.D., L.G., P.S., and M. Luksza; writing – original draft, K.V. and F. Klein; writing – reviewing and editing, C.F., M.M., H.G., N.P., C.K., and M.K.; supervision; F. Klein, P.J.B., M. Laessig, T.F.S., and L.E.S.; funding acquisition, F. Klein, L.E.S., M.K., M. Laessig, and P.J.B.

DECLARATION OF INTERESTS

F. Klein, K.V., and H.G. are listed as inventors on a patent application that covers aspects of this work. F.K., C.K., and H.G. are listed as inventors on a patent application regarding neutralizing antibodies against SARS-related coronaviruses. All other authors declare no competing interests.

Received: September 28, 2021
Revised: November 8, 2021
Accepted: December 10, 2021
Published: December 18, 2021

REFERENCES

Andreano, E., Nicastri, E., Paciello, I., Pileri, P., Manganaro, N., Piccini, G., Manenti, A., Pantano, E., Kabanova, A., Troisi, M., et al. (2021). Extremely potent human monoclonal antibodies from COVID-19 convalescent patients. Cell *184*, 1821–1835.e16.

Barnes, C.O., Jette, C.A., Abernathy, M.E., Dam, K.A., Esswein, S.R., Gristick, H.B., Malyutin, A.G., Sharaf, N.G., Huey-Tubman, K.E., Lee, Y.E., et al. (2020). SARS-CoV-2 neutralizing antibody structures inform therapeutic strategies. Nature *588*, 682–687.

Cerutti, G., Guo, Y., Zhou, T., Gorman, J., Lee, M., Rapp, M., Reddem, E.R., Yu, J., Bahna, F., Bimela, J., et al. (2021). Potent SARS-CoV-2 neutralizing antibodies directed against spike N-terminal domain target a single supersite. Cell Host Microbe *29*, 819–833.e817.

Chen, E.C., Gilchuk, P., Zost, S.J., Suryadevara, N., Winkler, E.S., Cabel, C.R., Binshtein, E., Chen, R.E., Sutton, R.E., Rodriguez, J., et al. (2021a). Convergent antibody responses to the SARS-CoV-2 spike protein in convalescent and vaccinated individuals. Cell Rep. *36*, 109604.

Chen, P., Nirula, A., Heller, B., Gottlieb, R.L., Boscia, J., Morris, J., Huhn, G., Cardona, J., Mocherla, B., Stosor, V., et al.; BLAZE-1 Investigators (2021b). SARS-CoV-2 Neutralizing Antibody LY-CoV555 in Outpatients with Covid-19. N. Engl. J. Med. *384*, 229–237.

Choi, B., Choudhary, M.C., Regan, J., Sparks, J.A., Padera, R.F., Qiu, X., Solomon, I.H., Kuo, H.H., Boucau, J., Bowman, K., et al. (2020). Persistence and Evolution of SARS-CoV-2 in an Immunocompromised Host. N. Engl. J. Med. *383*, 2291–2293.

Corti, D., Purcell, L.A., Snell, G., and Veesler, D. (2021). Tackling COVID-19 with neutralizing monoclonal antibodies. Cell *184*, 3086–3108.

Crawford, K.H.D., Eguia, R., Dingens, A.S., Loes, A.N., Malone, K.D., Wolf, C.R., Chu, H.Y., Tortorici, M.A., Veesler, D., Murphy, M., et al. (2020). Protocol and Reagents for Pseudotyping Lentiviral Particles with SARS-CoV-2 Spike Protein for Neutralization Assays. Viruses *12*, 513.

Cui, J., Li, F., and Shi, Z.L. (2019). Origin and evolution of pathogenic coronaviruses. Nat. Rev. Microbiol. *17*, 181–192.

Dejnirattisai, W., Zhou, D., Ginn, H.M., Duyvesteyn, H.M.E., Supasa, P., Case, J.B., Zhao, Y., Walter, T.S., Mentzer, A.J., Liu, C., et al. (2021). The antigenic anatomy of SARS-CoV-2 receptor binding domain. Cell *184*, 2183–2200.e2122.

Dong, E., Du, H., and Gardner, L. (2020). An interactive web-based dashboard to track COVID-19 in real time. Lancet Infect. Dis. *20*, 533–534.

Dougan, M., Nirula, A., Azizad, M., Mocherla, B., Gottlieb, R.L., Chen, P., Hebert, C., Perry, R., Boscia, J., Heller, B., et al.; BLAZE-1 Investigators (2021). Bamlanivimab plus Etesevimab in Mild or Moderate Covid-19. N. Engl. J. Med. *385*, 1382–1392.

Elbe, S., and Buckland-Merrett, G. (2017). Data, disease and diplomacy: GISAID's innovative contribution to global health. Glob Chall *1*, 33–46.

Emsley, P., Lohkamp, B., Scott, W.G., and Cowtan, K. (2010). Features and development of Coot. Acta Crystallogr. D Biol. Crystallogr. *66*, 486–501.

Gieselmann, L., Kreer, C., Ercanoglu, M.S., Lehnen, N., Zehner, M., Schommers, P., Potthoff, J., Gruell, H., and Klein, F. (2021). Effective

high-throughput isolation of fully human antibodies targeting infectious pathogens. Nat. Protoc. *16*, 3639–3671.

Halwe, S., Kupke, A., Vanshylla, K., Liberta, F., Gruell, H., Zehner, M., Rohde, C., Krähling, V., Gellhorn Serra, M., Kreer, C., et al. (2021). Intranasal Administration of a Monoclonal Neutralizing Antibody Protects Mice against SARS-CoV-2 Infection. Viruses *13*, 1498.

Hansen, J., Baum, A., Pascal, K.E., Russo, V., Giordano, S., Wloga, E., Fulton, B.O., Yan, Y., Koon, K., Patel, K., et al. (2020). Studies in humanized mice and convalescent humans yield a SARS-CoV-2 antibody cocktail. Science *369*, 1010–1014.

Harvey, W.T., Carabelli, A.M., Jackson, B., Gupta, R.K., Thomson, E.C., Harrison, E.M., Ludden, C., Reeve, R., Rambaut, A., Peacock, S.J., and Robertson, D.L.; COVID-19 Genomics UK (COG-UK) Consortium (2021). SARS-CoV-2 variants, spike mutations and immune escape. Nat. Rev. Microbiol. *19*, 409–424.

Hillus, D., Schwarz, T., Tober-Lau, P., Vanshylla, K., Hastor, H., Thibeault, C., Jentzsch, S., Helbig, E.T., Lippert, L.J., Tscheak, P., et al.; EICOV/COVIM Study Group (2021). Safety, reactogenicity, and immunogenicity of homologous and heterologous prime-boost immunisation with ChAdOx1 nCoV-19 and BNT162b2: a prospective cohort study. Lancet Respir. Med. *9*, 1255–1265.

Hoang, D.T., Chernomor, O., von Haeseler, A., Minh, B.Q., and Vinh, L.S. (2018). UFBoot2: Improving the Ultrafast Bootstrap Approximation. Mol. Biol. Evol. *35*, 518–522.

Hodcroft, E.B., Zuber, M., Nadeau, S., Vaughan, T.G., Crawford, K.H.D., Althaus, C.L., Reichmuth, M.L., Bowen, J.E., Walls, A.C., Corti, D., et al.; SeqCOVID-SPAIN consortium (2021). Spread of a SARS-CoV-2 variant through Europe in the summer of 2020. Nature *595*, 707–712.

Hoffmann, M., Kleine-Weber, H., Schroeder, S., Kruger, N., Herrler, T., Erichsen, S., Schiergens, T.S., Herrler, G., Wu, N.H., Nitsche, A., et al. (2020a). SARS-CoV-2 Cell Entry Depends on ACE2 and TMPRSS2 and Is Blocked by a Clinically Proven Protease Inhibitor. Cell *181*, 271–280.e278.

Hoffmann, M., Kleine-Weber, H., Schroeder, S., Krüger, N., Herrler, T., Erichsen, S., Schiergens, T.S., Herrler, G., Wu, N.H., Nitsche, A., et al. (2020b). SARS-CoV-2 Cell Entry Depends on ACE2 and TMPRSS2 and Is Blocked by a Clinically Proven Protease Inhibitor. Cell *181*, 271–280.e8.

Hoffmann, M., Hofmann-Winkler, H., Krüger, N., Kempf, A., Nehlmeier, I., Graichen, L., Arora, P., Sidarovich, A., Moldenhauer, A.S., Winkler, M.S., et al. (2021). SARS-CoV-2 variant B.1.617 is resistant to bamlanivimab and evades antibodies induced by infection and vaccination. Cell Rep. *36*, 109415.

Hsieh, C.L., Goldsmith, J.A., Schaub, J.M., DiVenere, A.M., Kuo, H.C., Javanmardi, K., Le, K.C., Wrapp, D., Lee, A.G., Liu, Y., et al. (2020). Structure-based design of prefusion-stabilized SARS-CoV-2 spikes. Science *369*, 1501–1505.

Ju, B., Zhang, Q., Ge, J., Wang, R., Sun, J., Ge, X., Yu, J., Shan, S., Zhou, B., Song, S., et al. (2020). Human neutralizing antibodies elicited by SARS-CoV-2 infection. Nature *584*, 115–119.

Katoh, K., and Standley, D.M. (2013). MAFFT multiple sequence alignment software version 7: improvements in performance and usability. Mol. Biol. Evol. *30*, 772–780.

Khoury, D.S., Cromer, D., Reynaldi, A., Schlub, T.E., Wheatley, A.K., Juno, J.A., Subbarao, K., Kent, S.J., Triccas, J.A., and Davenport, M.P. (2021). Neutralizing antibody levels are highly predictive of immune protection from symptomatic SARS-CoV-2 infection. Nat. Med. *27*, 1205–1211.

Kowarz, E., Löscher, D., and Marschalek, R. (2015). Optimized Sleeping Beauty transposons rapidly generate stable transgenic cell lines. Biotechnol. J. *10*, 647–653.

Krammer, F. (2020). SARS-CoV-2 vaccines in development. Nature *586*, 516–527.

Kreer, C., Döring, M., Lehnen, N., Ercanoglu, M.S., Gieselmann, L., Luca, D., Jain, K., Schommers, P., Pfeifer, N., and Klein, F. (2020a). openPrimeR for multiplex amplification of highly diverse templates. J. Immunol. Methods *480*, 112752.

Kreer, C., Zehner, M., Weber, T., Ercanoglu, M.S., Gieselmann, L., Rohde, C., Halwe, S., Korenkov, M., Schommers, P., Vanshylla, K., et al. (2020b). Longitudinal Isolation of Potent Near-Germline SARS-CoV-2-Neutralizing Antibodies from COVID-19 Patients. Cell *182*, 843–854.e812.

Liebschner, D., Afonine, P.V., Urzhumtsev, A.G., and Adams, P.D. (2020). Implementation of the riding hydrogen model in CCTBX to support the next generation of X-ray and neutron joint refinement in Phenix. Methods Enzymol. *634*, 177–199.

Liu, L., Wang, P., Nair, M.S., Yu, J., Rapp, M., Wang, Q., Luo, Y., Chan, J.F., Sahi, V., Figueroa, A., et al. (2020). Potent neutralizing antibodies against multiple epitopes on SARS-CoV-2 spike. Nature *584*, 450–456.

Liu, Z., VanBlargan, L.A., Bloyet, L.M., Rothlauf, P.W., Chen, R.E., Stumpf, S., Zhao, H., Errico, J.M., Theel, E.S., Liebeskind, M.J., et al. (2021). Identification of SARS-CoV-2 spike mutations that attenuate monoclonal and serum antibody neutralization. Cell Host Microbe *29*, 477–488.e474.

Lopez Bernal, J., Andrews, N., Gower, C., Gallagher, E., Simmons, R., Thelwall, S., Stowe, J., Tessier, E., Groves, N., Dabrera, G., et al. (2021). Effectiveness of Covid-19 Vaccines against the B.1.617.2 (Delta) Variant. N. Engl. J. Med. *385*, 585–594.

Mastronarde, D.N. (2005). Automated electron microscope tomography using robust prediction of specimen movements. J. Struct. Biol. *152*, 36–51.

McCallum, M., De Marco, A., Lempp, F.A., Tortorici, M.A., Pinto, D., Walls, A.C., Beltramello, M., Chen, A., Liu, Z., Zatta, F., et al. (2021). N-terminal domain antigenic mapping reveals a site of vulnerability for SARS-CoV-2. Cell *184*, 2332–2347.e2316.

Minh, B.Q., Schmidt, H.A., Chernomor, O., Schrempf, D., Woodhams, M.D., von Haeseler, A., and Lanfear, R. (2020). IQ-TREE 2: New Models and Efficient Methods for Phylogenetic Inference in the Genomic Era. Mol. Biol. Evol. *37*, 1530–1534.

Muecksch, F., Weisblum, Y., Barnes, C.O., Schmidt, F., Schaefer-Babajew, D., Wang, Z., Lorenzi, J.C.C., Flyak, A.I., DeLaitsch, A.T., Huey-Tubman, K.E., et al. (2021). Affinity maturation of SARS-CoV-2 neutralizing antibodies confers potency, breadth, and resilience to viral escape mutations. Immunity *54*, 1853–1868.e7.

Nielsen, S.C.A., Yang, F., Jackson, K.J.L., Hoh, R.A., Roltgen, K., Jean, G.H., Stevens, B.A., Lee, J.Y., Rustagi, A., Rogers, A.J., et al. (2020). Human B Cell Clonal Expansion and Convergent Antibody Responses to SARS-CoV-2. Cell Host Microbe *28*, 516–525.e515.

O'Brien, M.P., Forleo-Neto, E., Musser, B.J., Isa, F., Chan, K.C., Sarkar, N., Bar, K.J., Barnabas, R.V., Barouch, D.H., Cohen, M.S., et al.; Covid-19 Phase 3 Prevention Trial Team (2021). Subcutaneous REGEN-COV Antibody Combination to Prevent Covid-19. N. Engl. J. Med. *385*, 1184–1195.

Ozawa, T., Kishi, H., and Muraguchi, A. (2006). Amplification and analysis of cDNA generated from a single cell by 5′-RACE: application to isolation of antibody heavy and light chain variable gene sequences from single B cells. Biotechniques *40*, 469–470, 472, 474 passim.

Pallesen, J., Wang, N., Corbett, K.S., Wrapp, D., Kirchdoerfer, R.N., Turner, H.L., Cottrell, C.A., Becker, M.M., Wang, L., Shi, W., et al. (2017). Immunogenicity and structures of a rationally designed prefusion MERS-CoV spike antigen. Proc. Natl. Acad. Sci. USA *114*, E7348–E7357.

Pettersen, E.F., Goddard, T.D., Huang, C.C., Couch, G.S., Greenblatt, D.M., Meng, E.C., and Ferrin, T.E. (2004). UCSF Chimera–a visualization system for exploratory research and analysis. J. Comput. Chem. *25*, 1605–1612.

Piccoli, L., Park, Y.J., Tortorici, M.A., Czudnochowski, N., Walls, A.C., Beltramello, M., Silacci-Fregni, C., Pinto, D., Rosen, L.E., Bowen, J.E., et al. (2020). Mapping Neutralizing and Immunodominant Sites on the SARS-CoV-2 Spike Receptor-Binding Domain by Structure-Guided High-Resolution Serology. Cell *183*, 1024–1042.e21.

Pinto, D., Park, Y.J., Beltramello, M., Walls, A.C., Tortorici, M.A., Bianchi, S., Jaconi, S., Culap, K., Zatta, F., De Marco, A., et al. (2020). Cross-neutralization of SARS-CoV-2 by a human monoclonal SARS-CoV antibody. Nature *583*, 290–295.

Pinto, D., Sauer, M.M., Czudnochowski, N., Low, J.S., Tortorici, M.A., Housley, M.P., Noack, J., Walls, A.C., Bowen, J.E., Guarino, B., et al. (2021). Broad

betacoronavirus neutralization by a stem helix-specific human antibody. Science *373*, 1109–1116.

Planas, D., Veyer, D., Baidaliuk, A., Staropoli, I., Guivel-Benhassine, F., Rajah, M.M., Planchais, C., Porrot, F., Robillard, N., Puech, J., et al. (2021). Reduced sensitivity of SARS-CoV-2 variant Delta to antibody neutralization. Nature *596*, 276–280.

Punjani, A., Rubinstein, J.L., Fleet, D.J., and Brubaker, M.A. (2017). cryoSPARC: algorithms for rapid unsupervised cryo-EM structure determination. Nat. Methods *14*, 290–296.

Robbiani, D.F., Gaebler, C., Muecksch, F., Lorenzi, J.C.C., Wang, Z., Cho, A., Agudelo, M., Barnes, C.O., Gazumyan, A., Finkin, S., et al. (2020). Convergent antibody responses to SARS-CoV-2 in convalescent individuals. Nature *584*, 437–442.

Rogers, T.F., Zhao, F., Huang, D., Beutler, N., Burns, A., He, W.T., Limbo, O., Smith, C., Song, G., Woehl, J., et al. (2020). Isolation of potent SARS-CoV-2 neutralizing antibodies and protection from disease in a small animal model. Science *369*, 956–963.

Rydyznski Moderbacher, C., Ramirez, S.I., Dan, J.M., Grifoni, A., Hastie, K.M., Weiskopf, D., Belanger, S., Abbott, R.K., Kim, C., Choi, J., et al. (2020). Antigen-Specific Adaptive Immunity to SARS-CoV-2 in Acute COVID-19 and Associations with Age and Disease Severity. Cell *183*, 996–1012.e19.

Sagulenko, P., Puller, V., and Neher, R.A. (2018). TreeTime: Maximum-likelihood phylodynamic analysis. Virus Evol. *4*, vex042.

Sauer, M.M., Tortorici, M.A., Park, Y.J., Walls, A.C., Homad, L., Acton, O.J., Bowen, J.E., Wang, C., Xiong, X., de van der Schueren, W., et al. (2021). Structural basis for broad coronavirus neutralization. Nat. Struct. Mol. Biol. *28*, 478–486.

Song, G., He, W., Callaghan, S., Anzanello, F., Huang, D., Ricketts, J., Torres, J.L., Beutler, N., Peng, L., Vargas, S., et al. (2021). Cross-reactive serum and memory B-cell responses to spike protein in SARS-CoV-2 and endemic coronavirus infection. Nat. Comm. *12*, 2938.

Starr, T.N., Czudnochowski, N., Liu, Z., Zatta, F., Park, Y.J., Addetia, A., Pinto, D., Beltramello, M., Hernandez, P., Greaney, A.J., et al. (2021). SARS-CoV-2 RBD antibodies that maximize breadth and resistance to escape. Nature *597*, 97–102.

Thompson, M.G., Burgess, J.L., Naleway, A.L., Tyner, H., Yoon, S.K., Meece, J., Olsho, L.E.W., Caban-Martinez, A.J., Fowlkes, A.L., Lutrick, K., et al. (2021). Prevention and Attenuation of Covid-19 with the BNT162b2 and mRNA-1273 Vaccines. N. Engl. J. Med. *385*, 320–329.

Tiller, T., Meffre, E., Yurasov, S., Tsuiji, M., Nussenzweig, M.C., and Wardemann, H. (2008). Efficient generation of monoclonal antibodies from single human B cells by single cell RT-PCR and expression vector cloning. J. Immunol. Methods *329*, 112–124.

U.S. Department of Health & Human Services (2021). Pause in the Distribution of bamlanivimab/etesevimab. https://www.phe.gov/emergency/events/COVID19/investigation-MCM/Bamlanivimab-etesevimab/Pages/bamlanivimab-etesevimab-distribution-pause.aspx.

Vanshylla, K., Di Cristanziano, V., Kleipass, F., Dewald, F., Schommers, P., Gieselmann, L., Gruell, H., Schlotz, M., Ercanoglu, M.S., Stumpf, R., et al. (2021). Kinetics and correlates of the neutralizing antibody response to SARS-CoV-2 infection in humans. Cell Host Microbe *29*, 917–929.e4.

Volz, E., Hill, V., McCrone, J.T., Price, A., Jorgensen, D., O'Toole, A., Southgate, J., Johnson, R., Jackson, B., Nascimento, F.F., et al. (2021). Evaluating the Effects of SARS-CoV-2 Spike Mutation D614G on Transmissibility and Pathogenicity. Cell *184*, 64–75.e11.

von Boehmer, L., Liu, C., Ackerman, S., Gitlin, A.D., Wang, Q., Gazumyan, A., and Nussenzweig, M.C. (2016). Sequencing and cloning of antigen-specific antibodies from mouse memory B cells. Nat. Protoc. *11*, 1908–1923.

Walls, A.C., Park, Y.J., Tortorici, M.A., Wall, A., McGuire, A.T., and Veesler, D. (2020). Structure, Function, and Antigenicity of the SARS-CoV-2 Spike Glycoprotein. Cell *181*, 281–292.e6.

Wang, P., Nair, M.S., Liu, L., Iketani, S., Luo, Y., Guo, Y., Wang, M., Yu, J., Zhang, B., Kwong, P.D., et al. (2021). Antibody resistance of SARS-CoV-2 variants B.1.351 and B.1.1.7. Nature *593*, 130–135.

Weinreich, D.M., Sivapalasingam, S., Norton, T., Ali, S., Gao, H., Bhore, R., Musser, B.J., Soo, Y., Rofail, D., Im, J., et al.; Trial Investigators (2021). REGN-COV2, a Neutralizing Antibody Cocktail, in Outpatients with Covid-19. N. Engl. J. Med. *384*, 238–251.

Weisblum, Y., Schmidt, F., Zhang, F., DaSilva, J., Poston, D., Lorenzi, J.C., Muecksch, F., Rutkowska, M., Hoffmann, H.H., Michailidis, E., et al. (2020). Escape from neutralizing antibodies by SARS-CoV-2 spike protein variants. eLife *9*, e61312.

Williamson, E.J., Walker, A.J., Bhaskaran, K., Bacon, S., Bates, C., Morton, C.E., Curtis, H.J., Mehrkar, A., Evans, D., Inglesby, P., et al. (2020). Factors associated with COVID-19-related death using OpenSAFELY. Nature *584*, 430–436.

Wu, N.C., Yuan, M., Liu, H., Lee, C.D., Zhu, X., Bangaru, S., Torres, J.L., Caniels, T.G., Brouwer, P.J.M., van Gils, M.J., et al. (2020). An Alternative Binding Mode of IGHV3-53 Antibodies to the SARS-CoV-2 Receptor Binding Domain. Cell Rep. *33*, 108274.

Ye, J., Ma, N., Madden, T.L., and Ostell, J.M. (2013). IgBLAST: an immunoglobulin variable domain sequence analysis tool. Nucleic Acids Res. *41*, W34-40.

Yuan, M., Liu, H., Wu, N.C., Lee, C.D., Zhu, X., Zhao, F., Huang, D., Yu, W., Hua, Y., Tien, H., et al. (2020). Structural basis of a shared antibody response to SARS-CoV-2. Science *369*, 1119–1123.

Yuan, M., Huang, D., Lee, C.D., Wu, N.C., Jackson, A.M., Zhu, X., Liu, H., Peng, L., van Gils, M.J., Sanders, R.W., et al. (2021). Structural and functional ramifications of antigenic drift in recent SARS-CoV-2 variants. Science *373*, 818–823.

Zohar, T., and Alter, G. (2020). Dissecting antibody-mediated protection against SARS-CoV-2. Nat. Rev. Immunol. *20*, 392–394.

Zost, S.J., Gilchuk, P., Chen, R.E., Case, J.B., Reidy, J.X., Trivette, A., Nargi, R.S., Sutton, R.E., Suryadevara, N., Chen, E.C., et al. (2020). Rapid isolation and profiling of a diverse panel of human monoclonal antibodies targeting the SARS-CoV-2 spike protein. Nat. Med. *26*, 1422–1427.

STAR★METHODS

KEY RESOURCES TABLE

REAGENT or RESOURCE	SOURCE	IDENTIFIER
Antibodies		
APC Mouse Anti-Human IgG; Clone G18-145	BD Biosciences	Catalog# 550931; RRID: AB_398478
Alexa Fluor® 700 Mouse Anti-Human CD20; Clone 2H7	BD Biosciences	Catalog# 560631; RRID: AB_1727447
FITC Mouse Anti-Human IgM; Clone G20-127	BD Biosciences	Catalog# 555782; RRID: AB_396117
PE Mouse Anti-Human CD27; Clone M-T271	BD Biosciences	Catalog# 560985; RRID: AB_10563213
HRP-conjugated polyclonal goat anti-human IgG	Southern Biotech	Catalog# 2040-05; RRID: AB_2795644
Ultra-LEAF™ Purified anti-human CD28 Antibody	Biolegend	Catalog# 302934; RRID: AB_11148949
Brilliant Violet 605™ anti-human CD3 Antibody; Clone UCTH1	Biolegend	Catalog# 300460; RRID: AB_2564380
Alexa Fluor® 700 anti-human CD8a Antibody; Clone RPA-T8	Biolegend	Catalog# 301028; RRID: AB_493745
APC/Fire™ 750 anti-human CD4 Antibody; Clone RPA-T4	Biolegend	Catalog# 300560; RRID: AB_2629693
Brilliant Violet 785™ anti-human CD45RA Antibody; Clone HI-100	Biolegend	Catalog# 304140; RRID: AB_2563816
Brilliant Violet 650™ anti-human CD27 Antibody; Clone O323	Biolegend	Catalog# 302828; RRID: AB_2562096
Brilliant Violet 421™ anti-human CD137 (4-1BB) Antibody; Clone 4B4-1	Biolegend	Catalog# 309820; RRID: AB_2563830
FITC anti-human CD197 (CCR7) Antibody; Clone G043H7	Biolegend	Catalog# 353216; RRID: AB_10916386
APC anti-human CD69 Antibody; Clone FN50	Biolegend	Catalog# 310910; RRID: AB_314845
PE/Dazzle™ 594 anti-human CD154 Antibody; Clone 24-31	Biolegend	Catalog# 310840; RRID: AB_2566245
PE/Cyanine7 anti-human IFN-γ Antibody; Clone 4S.B3	Biolegend	Catalog# 502528; RRID: AB_2123323
PE anti-human CD185 (CXCR5) Antibody; Clone J252D4	Biolegend	Catalog# 356904; RRID: AB_2561813
S309 monoclonal antibody	Pinto et al., 2020	N/A
C102 monoclonal antibody	Robbiani et al., 2020	N/A
Fab2-36 monoclonal antibody	Liu et al., 2020	N/A
P2B-2F6 monoclonal antibody	Ju et al., 2020	N/A
REGN-10987 monoclonal antibody	Hansen et al., 2020	N/A
REGN-10989 monoclonal antibody	Hansen et al., 2020	N/A
DZIF-10c monoclonal antibody	(Halwe et al., 2021) (Kreer et al., 2020b)	N/A
IgG from donors R40, R121, R200, R259, R39, R410, R568, R616, R849	Vanshylla et al., 2021 and this study	N/A
IgA from donors R40, R121, R200, R259, R39, R410, R568, R616, R849	This study	N/A
Monoclonal antibodies from donors R40, R121, R200, R259, R39, R410, R568, R616, R849	This study	N/A
Bacterial and virus strains		
SARS-CoV-2 CoV2-P3 authentic virus	Vanshylla et al., 2021	N/A
SARS-2-S Wu01 pseudovirus	Vanshylla et al., 2021	N/A
SARS-2-S SARS-1 pseudovirus	This study	N/A
SARS-2-S WiV-1 pseudovirus	This study	N/A
SARS-2-S B.1 variant pseudovirus	Vanshylla et al., 2021	N/A
SARS-2-S B.1.1.7, B.1.351, B.1.429, B.1.617 and B.1.617.2 variants pseudovirus	This study	N/A

(*Continued on next page*)

Continued

REAGENT or RESOURCE	SOURCE	IDENTIFIER
SARS-2-S B.1 variants with RBD mutations: R346S; Q414H; K417E; N439K; N440K; K444Q; V445A; G446V; Y453F; G476S; S477N; T478K; E484K; F486V; F490S; Q493R; Q493K; S494P and N501Y pseudovirus	This study	N/A
Biological samples		
Plasma/serum from convalescent donors	Vanshylla et al., 2021 and this study	N/A
PBMCs from convalescent donors	Vanshylla et al., 2021 and this study	N/A
Chemicals, peptides, and recombinant proteins		
FuGENE® 6 Transfection Reagent	Promega	Catalog# E2691
Adenosine 5′-triphosphate disodium salt hydrate ATP	Sigma-Aldrich	Catalog# A2383-10G
Coenzyme A sodium salt hydrate,cofactor for acyl transfer	Sigma-Aldrich	Catalog# C3144-500MG
Igepal® CA-630 for molecular biology	Sigma-Aldrich	Catalog# I8896-100ML
D-Luciferin, Sodium Salt	ZellBio	Catalog# LUCNA-1G
Protein G Sepharose® 4 Fast Flow	Sigma-Aldrich	Catalog# GE17-0618-05
Peptide M Agarose	Invivogen	Catalog# gel-pdm-2
DAPI (4',6-Diamidino-2-Phenylindole, Dihydrochloride)	Thermo Fisher	Catalog# D1306
FreeStyle™ 293 Expression Medium	Thermo Fisher	Catalog# 12338018
RNaseOUT	Thermo Fisher	Catalog# 10777-019
RNasin	Promega	Catalog# N2515
DTT (Superscript IV Kit)	Thermo Fisher	Catalog# 18090050
Random Hexamer Primer	Thermo Fisher	Catalog# S0142
NP-40	Thermo Fisher	Catalog# 85124
5x RT Buffer (Superscript IV Kit)	Thermo Fisher	Catalog# 18090050
dNTPs	Thermo Fisher	Catalog# R1122
Superscript IV	Thermo Fisher	Catalog# 18090050
Platinum™ Taq polymerase	Thermo Fisher	Catalog# 10-966-026
Platinum™ Taq Green Hot Start DNA Polymerase	Thermo Fisher	Catalog# 11966034
Q5 Hot Start High Fidelity DNA Polymerase	NEB	Catalog# M0493L
Branched Polyethylenimine, 25 kDa	Sigma-Aldrich	Catalog# 408727
Puromycin	Sigma	Catalog# P4512
Doxycyclin	Sigma	Catalog# D3447
Strep-Tactin®XT 4Flow® high capacity resin	IBA Lifesciences	Catalog# 2-5030-500
Biotin Blocking Buffer	IBA Lifesciences	Catalog# 2-0501-002
ABTS Substrate Solution	Thermo Fisher	Catalog# 002024
Tween-20	Carl Roth	Catalog# 9127.20
EDTA 0.5 M, pH 8.0, RNase-free	Thermo Fisher	Catalog# AM9260G
HRP-conjugated Streptavidin	Thermo Fisher	Catalog# 21130
Crystallized Papain	Sigma Aldrich	Catalog# P3125
Octyl Maltoside, Fluorinated, Anagrade	Anatrace	Catalog# O310F
Pierce™ Universal Nuclease for Cell Lysis	Thermo Fisher	Catalog# 88702
SEB (Staphylococcal enterotoxin B from Staphylococcus aureus)	Merck/ Sigma-Aldrich	Catalog# 11100-45-1
eBioscience™ Brefeldin A-Lösung (1000x)	Thermo Fisher	Catalog# 00-4506-51
Dimethylsulfoxid	Sigma	Catalog# D4540
Zombie UV™ Fixable Viability Kit	Biolegend	Catalog# 423108
Human TruStain FcX Fc Receptor Blocking Solution	Biolegend	Catalog# 422302
eBioscience™ Foxp3/Transcription Factor Staining Buffer Set	Invitrogen	Catalog# 00-5523-00

(*Continued on next page*)

Continued

REAGENT or RESOURCE	SOURCE	IDENTIFIER
PepMix™ SARS-CoV-2 (Spike SUB1), Mix of 166 peptides (15mers, overlap 11)	JPT	Catalog# PM-WCPV-S-SU1-1
PepMix™ SARS-CoV-2 (Spike SUB2) Mix of 145 peptides (15mers, overlap 11)	JPT	Catalog# PM-WCPV-S-SU2-1
SARS-CoV-2 HexaPro bait protein	Jason McLellan lab; Hsieh et al., 2020	N/A
SARS-CoV-2 S1 domain protein for ELISA	This study	N/A
SARS-CoV-2 RBD domain protein for ELISA	This study	N/A
SARS-CoV-2 NTD domain protein for ELISA	This study	N/A
SARS-CoV-2 S2 domain protein for ELISA	This study	N/A
SARS-CoV-2 HexaPro trimer for ELISA	This study	N/A
SARS-CoV-1 spike trimer for ELISA	This study	N/A
MERS-CoV trimer for ELISA	This study	N/A
HCoV-HKU1 spike trimer for ELISA	This study	N/A
HCoV-OC43 spike trimer for ELISA	This study	N/A
Critical commercial assays		
NOVA Lite HEp-2 ANA Kit	Inova Diagnostics	Catalog# 708100
Q5® Site-Directed Mutagenesis Kit	NEB	Catalog# E0554
NEBuilder® HiFi DNA Assembly	NEB	Catalog# E2621S
DyLight 488 Antibody Labeling Kit	Thermo Fisher	Catalog# 53024
DyLight 650 Antibody Labeling Kit	Thermo Fisher	Catalog# 84535
Deposited data		
R40-1G8 spike structure coordinates	Protein Data Bank	PDB ID 7SC1
R40-1G8 spike structure EM map	Microscopy Data Bank	EMDB 25008
Tested monoclonal antibodies antibody V-gene sequences from donors R40, R121, R200, R259, R39, R410, R568, R616, R849	This paper	GenBank accession # OL741060 - OL741311
Experimental models: Cell lines		
HEK293T-ACE2 cells	Jesse Bloom lab; Crawford et al., 2020	BEI Resources Catalog# NR-52511
VeroE6 cells	ATCC	Catalog# CRL-1586
HEK293T	ATCC	Catalog# CRL-11268
2936E	National research Council Canada	NRC file 11565
HEK293 EBNA	Invitrogen	Catalog# R620907
Expi293F cells	GIBCO	Catalog# A14527
Oligonucleotides		
5′ oPR-IGHV primer mix	Kreer et al., 2020a	N/A
5′ oPR-IGKV primer mix	Kreer et al., 2020a	N/A
5′ oPR-IGLV primer mix	Kreer et al., 2020a	N/A
3′ Cg-RT primer	Ozawa et al., 2006	N/A
3′ Cκ-543 primer	Tiller et al., 2008	N/A
3′ Cκ-494 primer	Tiller et al., 2008	N/A
3′ IgG internal	Tiller et al., 2008	N/A
3′ XhoI Cλ	Tiller et al., 2008	N/A
5′ SLIC-oPR-IGHV primer	Kreer et al., 2020a	N/A
5′ SLIC-oPR-IGKV primer	Kreer et al., 2020a	N/A
5′ SLIC-oPR-IGLV primer	Kreer et al., 2020a	N/A
3′ SLIC_IgG_HC_rev	(Kreer et al., 2020b)	N/A
3′ SLIC_KC_rev	(Kreer et al., 2020b)	N/A
3′ SLIC_LC_rev	(Kreer et al., 2020b)	N/A

(*Continued on next page*)

Continued

REAGENT or RESOURCE	SOURCE	IDENTIFIER
Random Hexamer Primer	Thermo Fisher	Catalog #SO142
Recombinant DNA		
Human antibody expression vectors (IgG1, Igκ, Igλ)	Tiller et al., 2008	N/A
Human antibody expression vectors (IgG1, Igκ, Igλ) with V-gene antibody sequences from donors R40, R121, R200, R259, R39, R410, R568, R616, R849	This study	N/A
pHDM-tat1b	Jesse Bloom lab; Crawford et al., 2020	N/A
pHDM-Hgpm2	Jesse Bloom lab; Crawford et al., 2020	N/A
pRC-CMV-Rev1b	Jesse Bloom lab; Crawford et al., 2020	N/A
pHAGE-CMV-Luc2-IRES-ZsGreen-W	Jesse Bloom lab; Crawford et al., 2020	N/A
SARS-CoV-2 Wu01 codon optimized spike	(Hoffmann et al., 2020b)	N/A
pcDNA™3.1/V5-His TOPO™ SARS-2-S Wu01 spike	Vanshylla et al., 2021	N/A
pcDNA™3.1/V5-His TOPO™ SARS-2-S B.1 spike variant	Vanshylla et al., 2021	N/A
pcDNA™3.1/V5-His TOPO™ SARS-2-S B.1.1.7, B.1.351, B.1.429, B.1.617 and B.1.617.2 spike variants	This study	N/A
pcDNA™3.1/V5-His TOPO™ SARS-2-S B.1 variants with RBD mutations: R346S; Q414H; K417E; N439K; N440K; K444Q; V445A; G446V; Y453F; G476S; S477N; T478K; E484K; F486V; F490S; Q493R; Q493K; S494P and N501Y	This study	N/A
pCAGGS-SARS-CoV2-S-HexaPro spike	Jason McLellan lab; Hsieh et al., 2020	N/A
pCDNA3.1-SARS-CoV-1 spike	Jason McLellan lab	N/A
pCG1-WiV-1 spike	This study	N/A
pVRC-MERS-CoV spike	Jason McLellan lab; (Pallesen et al., 2017)	N/A
phCMV3-HCoV-HKU1 spike	Raiees Andrabi lab; (Song et al., 2021)	N/A
phCMV3- HCoV-OC43 spike	Raiees Andrabi lab; (Song et al., 2021)	N/A
Software and algorithms		
GraphPad PRISM, Version 7 and 9	GraphPad Software, Inc	https://www.graphpad.com
Geneious R10v10.0.9	Biomatters	https://www.geneious.com
Illustrator® CC 2018	Adobe	https://www.adobe.com
BertholdTech TriStar2S ICE, Version 1.0.9.5	Berthold Technologies	https://www.berthold.com/en
IgBLAST	Ye et al., 2013	N/A
SerialEM automated data collection software	Mastronarde, 2005	N/A
cryoSPARC v3.2	Punjani et al., 2017	N/A
Chimera visualization software	Pettersen et al., 2004	N/A
Coot molecular-graphics application	Emsley et al., 2010	N/A
Phenix	Liebschner et al., 2020	N/A
GISAID EpiCov database	Elbe and Buckland-Merrett, 2017	N/A
MAFFTv7.467	Katoh and Standley, 2013	N/A
IQTree	Minh et al., 2020	N/A
TreeTime	Sagulenko et al., 2018	N/A

(*Continued on next page*)

Continued

REAGENT or RESOURCE	SOURCE	IDENTIFIER
Other		
C102 spike structure	Protein Data Bank; Barnes et al., 2020	PDB ID 7K8M
C105 spike structure	Protein Data Bank; Barnes et al., 2020	PDB ID 6XCM
C002 spike structure	Protein Data Bank; Barnes et al., 2020	PDB ID 7K8T
CD19 MicroBeads, human	Miltenyi Biotec	Catalog# 130-050-301
Amicon Ultra-0.5 Centrifugal Filter Unit 10 kDa	Merck	Catalog# UFC501096
Amicon Ultra-0.5 Centrifugal Filter Unit Ultracel-30, 0.5 mL sample	Millipore Sigma	Catalog# UFC503096
Amicon® Ultra-4	Sigma-Aldrich	Catalog# UFC803096
Corning® 96-well EIA/RIA Easy Wash™ Clear Flat Bottom Polystyrene High Bind Microplate	Corning	Catalog# 3369
96-well Black Flat Bottom Polystyrene Not Treated Microplate	Corning	Catalog# 3628
96-well Clear Flat Bottom TC-treated Microplate	Corning	Catalog# 3915
NucleoSpin® 96 PCR Clean-up	Macherey-Nagel	Catalog# 740658.4
Q5® High-Fidelity 2X Master Mix,	NEB	Catalog# M0492S
EZ-Link Sulfo-NHS-Biotin	Thermo Fisher	Catalog# A39256
HiTrapTM MabSelect SuReTM	GE Healthcare Life Sciences	Catalog# 11-0034-94
Superdex 200 Increase 10/300 column	GE Healthcare Life Sciences	Catalog# 28-9909-44
QuantaFoil 300 mesh 1.2/1.3 grids	Electron Microscopy Sciences	Catalog# Q310CR1.3
PELCO easiGlow™ Glow system	Ted Pella	Catalog# 91000
Vitrobot Mark IV	Thermo Fisher	N/A
Leica DMI3000 B microscope	Leica	N/A
Sunrise™ microplate reader	Tecan	N/A
BertholdTech TriStar2S luminometer	Berthold Technologies	N/A
BD FACSAria Fusion™	Becton Dickinson	N/A
Krios G4 Cryo-Transmission Electron Microscope with Gatan K3 camera	Thermo Fisher	N/A

RESOURCE AVAILABILITY

Lead contact

Requests for resources and reagents should be directed to and will be fulfilled by the lead contact, Florian Klein (florian.klein@uk-koeln.de).

Materials availability

Request for reagents will be made available by the lead contact with a Material Transfer Agreement.

Data and code availability

- All data has been included in main figures or supplementary information.
- SARS-CoV-2 antibody sequences are available at GenBank with accession numbers OL741060 - OL741311. The atomic coordinate and 3D EM reconstruction for SARS-CoV-2 S 6P in complex with R40-1G8 Fab has been deposited in the Protein Data Bank (PDB) with PDB ID 7SC1 and the Electron Microscopy Data Bank (EMDB) with EMDB 25008, respectively.
- Any additional information required to reanalyze the data reported in this paper is available from the lead contact upon request.

EXPERIMENTAL MODEL AND SUBJECT DETAILS

Enrollment of human subjects and study design

Blood samples were collected from donors (for details please refer to Table S1) who gave their written consent under the protocols 20-1187 and 16-054, approved by the Institutional Review Board (IRB) of the University Hospital Cologne. The COVID-19 convalescent cohort of 963 individuals was previously described in detail (Vanshylla et al., 2021). Samples for single B cell analysis were collected from 5 male and 5 female participants (median age 43 years) at a median of 19 weeks post disease onset. Additional

samples for IgG/IgA neutralization and T cell analyses were obtained from 18 male and 13 female participants (median age 47 years) at a median of 7.4 weeks post disease onset. The COVID-19 convalescent donors tested SARS-CoV-2 positive between March and April 2020, and were not treated with SARS-CoV-2 monoclonal antibodies or received a COVID-19 vaccine prior to sample collection.

Cell lines

VeroE6 cells, HEK293T cells and 293T-ACE2 cells were maintained in DMEM (GIBCO) containing 10% FBS, 1% PS, 1mM L-Glutamine and 1mM Sodium pyruvate. Cells were grown on tissue culture treated T75 flask (Sarstedt) at 37°C and 5% CO_2. 293-6E cells were maintained at 37°C and 6% CO_2 in FreeStyle Expression Medium (Thermo Fisher) and kept under constant shaking at 110-120 rpm.

METHOD DETAILS

Processing of serum, plasma and whole blood samples

Blood samples were collected in Heparin syringes or EDTA monovette tubes (Sarstedt) and fractionated into plasma and peripheral blood mononuclear cell (PBMC) by density gradient centrifugation using Histopaque-1077 (Sigma). PBMCs were stored at −150°C. Plasma aliquots were stored at −80°C till use. Serum was collected from Serum-gel tubes (Sarstedt) by centrifugation and stored at −80°C till use.

Isolation of IgGs and IgAs from serum and plasma samples

For the isolation of total IgG, 0.5-1 mL plasma was heat inactivated for 45 min at 56°C and incubated with Protein G Sepharose 4 Fast Flow beads (GE Healthcare) at 4°C overnight. For isolation of IgA, 0.5 mL heat inactivated plasma was incubated with Peptide M Agarose beads (Invivogen) at 4°C overnight. On the next day, the beads were washed on chromatography columns (BioRad) and Protein G bound IgG or Peptide M bound IgA was eluted using 0.1M Glycine pH = 3 and immediately buffered with 1M Tris pH = 8. Buffer exchange to PBS (GIBCO) was performed using 30 kDa cut-off Amicon Ultra-15 columns (Millipore) and the purified IgG or IgA was stored at 4°C.

Single B cell sorting

Single B cell analyses were performed as previously described (Gieselmann et al., 2021). The SARS-CoV-2 variant called HexaPro, which has a pre-fusion spike confirmation (Hsieh et al., 2020) was used as bait protein for sorting spike-specific B cells from elite neutralizers using a 2-color sorting strategy. The HexaPro protein was labeled using the DyLight 488 or Dylight 650 antibody labeling kits (Thermo Fisher) as per manufacturer's protocol. B cells were enriched from the peripheral blood mononuclear cell (PBMC) fraction using the CD19 Microbeads kit (Miltenyi Biotec). Enriched B cells were stained with antibodies against human CD20, human IgG, DAPI, HexaPro-Dylight-488 and HexaPro-Dylight-650. B cells that were DAPI-negative, CD20-positive, IgG-positive, HexaPro-Dylight-488-positive and HexaPro-Dylight-650-positive were sorted onto 96 well plates containing sorting buffer comprised of 0.2 μL RNAsin (40U/μl Promega), 0.1 μL RNaseOut (40 U/μl Thermo Fisher), 0.2 μL 10X PBS, 0.4 μL DTT (100mM Promega) and 3.1 μL Nuclease free H_2O (Thermo Fisher). Sorts were done on a BD FACSAria Fusion cell sorter (Becton Dickinson) and sorted cells were frozen at −80°C until further processing.

Single cell cDNA production and PCR

Sorted single B cells were lysed at 65°C for 1 min with 0.75 μL Random Hexamer Primer (200 ng/μl Thermo Fisher), 0.5 μL NP-40 (10% Thermo Fisher), 0.15 μL RNaseOUT (100mM Thermo Fisher) and 5.6 μL Nuclease-free H_2O (Thermo Fisher). Thereafter, 2 μL Nuclease-free H_2O (Thermo Fisher), 3 μL 5X RT Buffer (Invitrogen), 0.5 μL dNTPs (25mM Thermo Fisher), 1 μL DTT (100mM Invitrogen), 0.1 μL RNAsin (40 U/μl Promega), 0.1 μL RNaseOUT (40 U/μl Thermo Fisher) and 0.25 μL Superscript IV (200 U/μl Invitrogen) were added and reverse transcription performed by incubating at RT for 10 min, 42°C for 10 min, 25°C for 10 min, 50°C for 10 min and 94°C for 5 min. Individual antibody sequences were amplified using semi-nested PCR. Heavy, kappa and lambda chains were simultaneously amplified in the 1st PCR using Platinum Taq DNA polymerase (Thermo Fisher) using the 5′ oPR-IGHV, oPR-IGKV and oPR-IGLV primer mix (Kreer et al., 2020a) along with the 3′ Cg-RT (Ozawa et al., 2006), 3′ Cκ 543 (Tiller et al., 2008) and 3′ Cκ 494 (Tiller et al., 2008). 1st PCR was run at 94°C for 1 min, 50 cycles of 94°C for 30 s, 57°C for 30 s, 72°C for 55 s and final extension at 72°C for 5 min. In the 2nd PCR, the antibody chains were amplified in separate reaction using primer pairs of 5′ oPR-IGHV + 3′ IgG internal (Tiller et al., 2008) (heavy chain), 5′ oPR-IGKV + 3′ Cκ 494 (kappa chain) and 5′ oPR-IGLV + 3′ XhoI Cλ (Tiller et al., 2008) (lambda chain). 2nd PCR was run at 94°C for 1 min, 50 cycles of 94°C for 30 s, 57°C for 30 s, 72°C for 45 s and final extension at 72°C for 5 min. 2nd PCR products were sequenced by Sanger sequencing for subsequent sequence analysis.

Antibody sequence analysis

Antibody sequence analysis was performed using a python-based in-house pipeline as previously described (Kreer et al., 2020b). B cell sequences with a minimum length of 240 nucleotides and a mean Phred score of >= 28 amino acids were annotated with IgBLAST (Ye et al., 2013) and trimmed from Framework region (FWR) 1 to the end of the J gene of the variable region. Base calls with Phred score of < 16 were masked and sequences with > 15 masked nucleotides, frameshifts or stop codons were excluded from further analyses. From these productive sequences, clonality was analyzed by grouping identical V genes, and the pairwise

Levenshtein distance of their CDRH3 was determined. Individual sequences were grouped into a clonal culster when they shared the same VH gene and the minimal CDRH3 identity (defined by Levenshtein distance in relation to the length of the shorter CDRH3) was >=75%. Sequences that remained unassigned after 20 rounds of randomized input were designated as being non-clonal. CDRH3 length was calculated based on IMGT numbering and % of sequences with a particular V-gene out of all sequences within an individual. Healthy reference shown in gray in Figure 2C. For the similarity network analysis in Figure 2D, B cells with the same VH gene from one individual was linked to a sequence from another individual when CDRH3 amino acid similarity (defined by Levenshtein distance in relation to the length of the shorter CDRH3) is >= 75%. Reference B cell heavy chain sequences in Figure 2 were derived from naive donors (Kreer et al., 2020b).

Antibody cloning for protein synthesis

For cloning of single B cell-derived antibodies, the 1st PCR product was used to amplify the variable regions for each antibody chain in separate reactions using the 5′ primers SLIC-oPR-IGHV, SLIC-oPR-IGKV and SLIC-oPR-IGLV (Kreer et al., 2020a) and 3′ primers SLIC_IgG_HC_rev, SLIC_KC_rev and SLIC_LC_rev (Kreer et al., 2020b) for heavy, kappa and lambda chain respectively. PCR was performed using the Q5 Hot Start High Fidelity DNA Polymerase (NEB) and run at 98°C for 30 s, 35 cycles of 98°C for 10 s, 72°C for 45 s and final extension at 72°C for 2 min. The PCR product was purified using the NucleoSpin® 96 PCR Clean-up kit (Macherey-Nagel) and cloned into the respective pIg expression vectors (pIgG1, pIgK, or pIgL) by restriction digest and SLIC assembly (von Boehmer et al., 2016).

Antibody synthesis

Antibodies were produced by transfection of 293-6E cells (National Research Council Canada) using branched polyethylenimine (PEI) 25kDa (Sigma-Aldrich) with 0.5 μg heavy chain plasmid and 0.5 μg light chain plasmid per 1 mL 293-6E culture. Cells were maintained at 37°C and 6% CO_2 FreeStyle 293 Expression Medium (Thermo Fisher) and 0.2% Penicillin/Streptomycin 7 days post transfection, the cell culture supernatant was harvested, filtered with a 0.45 μM Nalgene Rapid Flow filter (Thermo Fisher) and incubated overnight at 4°C with Protein G Sepharose 4 Fast Flow (GE Healthcare) overnight. Antibody bound Sepharose beads were washed on chromatography columns (BioRad) and antibodies were eluted using 0.1 M Glycine pH = 3 and immediately buffered in 1 M Tris pH = 8. Thereafter, buffer exchange to PBS was performed using 50 kDa Amicon Ultra-15 spin columns (Millipore) and the antibodies were stored at 4°C.

Cloning of SARS-CoV-2 spike variants

The codon optimized SARS-CoV-2 Wu01 spike (Hoffmann et al., 2020b) (EPI_ISL_406716) was cloned into pCDNA™3.1/V5-His-TOPO vector (Invitrogen). The D614G, 69-70 deletion and RBD mutants were generated by introducing the corresponding amino acid mutations using the Q5® Site-Directed Mutagenesis Kit (NEB) and per manufacturer's protocol. SARS-2-S RBD variants were generated in the B.1 background and included R346S; Q414H; K417E; N439K; N440K; K444Q; V445A; G446V; Y453F; G476S; S477N; T478K; E484K; F486V; F490S; Q493R; Q493K; S494P and N501Y. SARS-2-S variants B.1.1.7, B.1.351, B.1.429, B.1.617 and B.1.617.2 were generated by introducing the corresponding amino acid mutations (Figure S3) using PCR and HiFi assembly (NEBuilder® HiFi DNA Assembly Kit, New England Biolabs) of overlapping segments as per manufacturer's protocol.

Production of SARS-CoV pseudovirus particles

Pseudovirus particles were generated by co-transfection of individual plasmids encoding HIV-1 Tat, HIV-1 Gag/Pol, HIV-1 Rev, luciferase followed by an IRES and ZsGreen, and the SARS-CoV-2, (Crawford et al., 2020), SARS-CoV-1 or WiV-1 spike protein. In brief, HEK293T cells were transfected with the pseudovirus encoding plasmids using FuGENE® 6 Transfection Reagent (Promega). The virus culture supernatant was harvested at 48 h and 72 h post transfection and stored at −80°C until use. Each virus batch was titrated by infecting 293T-ACE2 and after a 48 h incubation period at 37°C and 5% CO_2, luciferase activity was determined after addition of luciferin/lysis buffer (10 mM MgCl2, 0.3 mM ATP, 0.5 mM Coenzyme A, 17 mM IGEPAL (all Sigma-Aldrich), and 1 mM D-Luciferin (GoldBio) in Tris-HCL) using a microplate reader (Berthold). Pseudovirus dilution resulting in a RLU of approximately 1000-fold in infected cells versus non-infected cells was used for neutralization assays.

Pseudovirus assay to determine IgG/plasma/serum neutralizing activity

For testing neutralizing activity of IgG or serum/plasma samples, serial dilutions of IgG or serum/plasma (heat inactivated at 56°C for 45 min) were co-incubated with pseudovirus supernatants for 1 h at 37°C prior to addition of 293T cells engineered to express ACE2 (Crawford et al., 2020). Following a 48 h incubation at 37°C and 5% CO_2, luciferase activity was determined using the reagents described above. After subtracting background relative luminescence units (RLUs) of non-infected cells, 50% inhibitory concentrations (IC_{50}s) were determined as the IgG concentrations resulting in a 50% RLU reduction compared to untreated virus control wells. 50% Inhibitory dose (ID_{50}) was determined as the serum dilution resulting in a 50% reduction in RLU compared to the untreated virus control wells. Each IgG and serum sample were measured in two independent experiments on different days and the average IC_{50} or ID_{50} values have been reported. For each run, a SARS-CoV-2 neutralizing monoclonal antibody was used as control to ensure consistent reproducibility in experiments carried out on different days. Assay specificity calculated using pre-COVID-19 samples was found to be 100%. IgG IC_{50} or serum/plasma ID_{50} values were calculated in GraphPad Prism 7.0 by plotting a dose response curve.

SARS-CoV-2 authentic virus neutralization assay

Authentic SARS-CoV-2 was previously grown out from a swab from Cologne using VeroE6 cells (Vanshylla et al., 2021). For the neutralization assay, dilutions of monoclonal IgG were co-incubated with the virus (1000-2000 $TCID_{50}$) for 1 h at 37°C prior to addition of VeroE6 cells in DMEM (GIBCO) containing 2% FBS, 1% PS, 1mM L-Glutamine and 1mM Sodium pyruvate. After 4 days of incubation at 37°C, 5% CO_2, neutralization was analyzed by observing cytopathic effects (CPE) using a brightfield microscope and the highest dilution well with no CPE was noted to be the IC_{100} for the antibody. All samples were measured in two independent experiments on separate days and the average IC_{100} from all measurements is reported.

SARS-CoV-2 T cell reactivity assay

To detect SARS-CoV-2 spike-specific T cells, an activation induced marker (AIM) assay was used. Frozen PBMCs were thawed in prewarmed RPMI 1640 supplemented with 10% FCS (Sigma-Aldrich), 1% Glutamax (GIBCO) and Pierce Universal Nuclease for Cell Lysis (ThermoFisher) and washed before resuspention in cRPMI (RPMI containing 10% heat-inactivated FCS (Sigma-Aldrich), 1% Penicillin-Streptomycin (Sigma-Aldrich), 1% Glutamax (GIBCO), 1% NEAA (Thermo Fisher), 1% HEPES (Thermo Fisher), 1% Sodium Pyruvate (Thermo Fisher) and rested for 5 h at 37°C and 5% CO2 in a humidified incubator. Live cells were counted on a MACSQuant Analyzer 16 (Miltenyi Biotec) with DAPI (Miltenyi Biotec) and seeded in 96 well U-bottom plates at 5×10^5 live cells per well in 100 μL in cRPMI. To stimulate cells, 1 μg/mL PepMix SARS-CoV-2 spike glycoprotein (JPT) peptide pool 1 (S1 domain) or 2 (S2 domain) in the presence of 1 μg/mL anti-CD28 antibody was added to up to six technical replicates per condition. Staphyoccocal enterotoxin B (SEB, Sigma-Aldrich) stimulated positive controls and negative controls using equivalent amount of DMSO and 1 μg/mL anti-CD28 antibody were included in parallel. Stimulated cells were incubated for 2 h before cytokine secretion inhibition with Brefeldin A (eBioscience). 19 h post stimulation, anti-human CXCR5 antibody was added to the culture for 30 min. Cells were then washed in PBS, technical replicates pooled and incubated with Zombie UV Live/Dead and Human TruStain FcX for 30 min at 4°C. Cells were then washed twice and incubated with the surface stain cocktail for 30 min at 4°C (all anti-human; CD45RA BV785, CD27 BV650, CCR7 FITC, CD69 APC and PD-1 eFluor506). Cells were permeabilized and fixed (eBioscience Foxp3/Transcription Factor Staining Buffer set) for 30 min at RT, washed and stained with the intracellular antibody cocktail for 30 min at 4°C (all anti-human; CD3 BV605, CD8 AF700, CD4 APC-Fire750, CD137 BV421, CD154 PE-Dazzle594, IFNg PE-Cy7). Cells were washed twice and acquired on a Cytoflex LX (Beckman Coulter) within 24 h of staining. Data were analyzed using FlowJo v10 (BD Bioscience). AIM+ CD4 T cells were defined by co-expression of CD137 and CD154 and frequencies calculated by background-subtraction of paired unstimulated controls. Researchers were blinded to grouping of samples during the experiment and data analysis. Antibody details can be found in the key resources table.

Production of coronavirus spike proteins

The following coronavirus regions were amplified from synthetic gene plasmids and cloned into modified Sleeping Beauty transposon expression vectors (Kowarz et al., 2015). Proteins used in ELISA included SARS-2 S1 domain: MN908947, A.A. 14-609, RRAR to GGGG, N-terminal BM40 signal peptide followed by a Twin strep tag, 83 kDa; SARS-2 S2 domain: MN908947, A.A. 686-1208, K986P, V987P, BM40 signal peptide; C-terminal Twin strep tag, 61 kDa; SARS-2 RBD domain: MN908947, A.A. 331-524, N-terminal Twin strep tag, 26 kDa; SARS-2 NTD domain: MN908947, A.A. 1-330, C-terminal Twin strep tag, 40 kDa; HexaPro spike trimer: MN908947, A.A. 1-1208, RRAR to GSAS, F817P, A892P, A899P, A942P, K986P, V987P, C-terminal T4 foldon followed by a Twin strep tag, 139 kDa; SARS-1 spike trimer: AAP13567, A.A. 18-1190, BM40 signal peptide, C-terminal T4 foldon – Twin strep tag, codon Optimized, 137 kDa; MERS spike trimer: AHE78097, A.A. 18-1291, RSVR to ASVG, V1060P, L1061P, BM40 signal peptide, C-terminal T4 foldon – Twin strep tag, 147 kDa ; HKU1 spike trimer: YP_173238, A.A. 1-1295, RRKRR to GSAG, A1071P, L1072P, C-terminal T4 foldon – Twin strep tag, 149 kDa; OC43 spike trimer: AAX84792, A.A. 1-1300, RRSRR to GSAS, A1078P, L1079P, C-terminal T4 foldon – Twin strep tag, 150 kDa. For recombinant protein production, stable HEK293 EBNA cell lines were generated employing the sleeping beauty transposon system (Kowarz et al., 2015). Briefly, expression constructs were co-transfected with a transposase plasmid (10:1) into the HEK293 EBNA cells, and after puromycin selection (3 μg/mL; Sigma), cells were expanded in triple flasks and protein production induced with doxycycline (0.5 μg/mL, Sigma). Supernatants of confluent cells were harvested every 3 days, filtered and recombinant proteins purified via Strep-Tactin®XT (IBA Lifescience, Göttingen, Germany) resin. Proteins were eluted with biotin containing TBS-buffer (IBA Lifescience, Göttingen, Germany), dialyzed against TBS-buffer, checked on an SDS-gel and aliquots stored at −80°C.

Detection of spike-specific reactivity by ELISA

For assessing binding reactivity, 2 μg/mL protein was coated overnight at 4°C on high binding 96-well assay plates (Corning). Proteins used were SARS-CoV-2 spike trimer (aa 1-1204), SARS-CoV-2 S1 monomer (aa 16-609), SARS-CoV-2 RBD monomer (aa 331-524), SARS-CoV-2 NTD monomer (aa 1-330), SARS-CoV-2 S2 monomer (aa 610-1208), SARS-1 spike trimer (aa 18-1190), MERS spike trimer (aa 18-1291), OC43 spike trimer (aa 1-1300), HKU1 spike trimer (aa 1-1295). Wells were washed at each step with washing buffer containing 0.05% Tween-20 (Carl Roth) in PBS. Uncoated sites were blocked with blocking buffer containing 3% milk powder (Carl Roth), 1 μM EDTA (Thermo Fisher) and 0.1% Tween-20 by incubating for 120 min at RT. After this, a dilution series of the samples, starting with a highest concentration of 1 mg/mL for total plasma IgG and 10 μg/mL for mAbs was added for 90 min at RT. For detection of binding signal from the primary antibody, goat anti-human IgG-HRP (Southern Biotech) was added for 60 min at RT. ABTS solution (Thermo Fisher) was added as substrate and the absorbance at 415 nm with reference at 695 nm was measured on the Sunrise microplate reader (Tecan). The optical density (OD) was used to plot binding curves and calculate area under curve (AUC) in GraphPad Prism 9.0.

Competition ELISA

For competition ELISA, 0.5 mg antibody was biotinylated with a 50X molar excess of biotin using the EZ-Link Sulfo-NHS-Biotin kit (Thermo Fisher) as per manufacturer's protocol. 2 μg/mL SARS-CoV-2 spike trimer (aa 1-1204) was coated on overnight at 4°C on high binding 96-well assay plates (Corning). Wells were washed at each step with washing buffer containing 0.05% Tween-20 (Carl Roth) in PBS. Uncoated sites were blocked with blocking buffer containing 3% milk powder (Carl Roth), 1 μM EDTA (Thermo Fisher) and 0.1% Tween-20 at RT for 120 min. After this, a dilution series of the samples to be tested, starting with a highest concentration of 40 μg/mL for mAbs was added for 60 min at RT. Following this, 0.4 μg/mL of the biotinylated antibody was added on top of the primary antibody for an additional 60 min at RT. For detection of binding signal from the biotinylated antibody, HRP-conjugated Streptavidin (Thermo Fisher) was added for 60 min at RT. ABTS solution (Thermo Fisher) was added as substrate and the absorbance at 415 nm with reference at 695 nm was measured on the Sunrise microplate reader (Tecan). The OD values were normalized to a negative control showing no competition in order to calculate the % competition and the non-biotinylated version of the same antibody was tested in parallel to confirm maximum competition (over 95%).

Hep-2 autoreactivity assay

HEp-2 cell autoreactivity assay was performed as per manufacturer's protocol using the NOVA Lite Hep-2 ANA kit (Inova Diagnostics) using 100 μg/mL of monoclonal antibody in DPBS. As a positive control, the Hep-2 cell-reactive HIV-1 neutralizing antibody 4E10 was included. Images were acquired using a Leica DMI3000 B microscope with 1500 ms exposure and a gain of 10. Images were processed in Adobe Photoshop and assembled in Adobe Illustrator CC 2018®.

Production of Fab fragments and spike protein and sample preparation for cryo-EM

The expression and purification of SARS-CoV-2 HexaPro (6P) stabilized S trimers (Hsieh et al., 2020) and antibody Fabs was carried out based on a previously published protocol (Muecksch et al., 2021). Briefly, Expi293F cells (GIBCO) were transiently transfected and supernatants used to purify protein using Ni^{2+}-NTA affinity size exclusion chromatography (SEC). SEC peak fractions were identified with SDS-PAGE and pooled and stored at 4°C. Fabs were generated with papain digestion from purified IgG at a 1:100 enzyme: IgG ratio by using crystallized papain (Sigma-Aldrich) in 50 mM sodium phosphate, 2mM EDTA, 10 mM L-cysteine and pH 7.4 for 30-60 min at 37°C. Fc fragments and undigested IgG were removed by applying digested products to a 1 mL HiTrap MabSelect SuRe column (GE Healthcare Life Sciences), and flow-through containing the cleaved Fabs was collected. SEC was done using a Superdex 200 Increase 10/300 column (GE Healthcare Life Sciences) in TBS to further purify the Fabs which were finally concentrated and stored at 4°C. SARS-CoV-2 S 6P trimer was mixed with purified R40-1G8 Fabs to a final concentration of 2 mg/mL with a 1.1:1 molar ratio Fab per SARS-CoV-2 S 6P protomer. The complex was incubated at room temperature for 30 min. QuantaFoil 300 mesh 1.2/1.3 grids (Electron Microscopy Sciences) were glow-discharged for 1 min at 20 mA using a PELCO easiGLOW (Ted Pella). Immediately before depositing 3 μL of the protein complex on to the glow-discharged grid, fluorinated octyl-maltoside (Anatrace) was added to the protein complex solution to a final concentration of 0.02% (w/v). The grids were blotted for 3 s with 0 blot force using Whatman No.1 filter paper at room temperature and 100% humidity and vitrified in 100% liquid ethane using Mark IV Vitrobot (Thermo Fisher).

Cryo-EM data collection, processing and refinement

Single-particle cryo-EM dataset for SARS-CoV-2 S 6P trimer in complex with R40-1G8 was collected using SerialEM automated data collection software (Mastronarde, 2005) on a 300 keV Titan Krios (Thermo Fisher) equipped with a K3 camera (Gatan). Detailed data processing workflow is outlined in Figure S5. 4,496 movies were recorded using a 3x3 beam image shift pattern with 3 exposures each hole with a pixel size of 0.416 Å in the superresolution mode. These cryo-EM movies were patch motion corrected with a binning factor of 2 and the CTF parameters were estimated using Patch CTF in cryoSPARC v3.2 (Punjani et al., 2017). Particles were picked using blob picker in cryoSPARC using a particle diameter of 100 to 200 Å, and movies and picked particles were inspected before extraction. A total of 840,417 particles were extracted and used to 2D classification. After discarding ice particles, the remaining 776,803 particles were used to generate four *ab initio* models. The particles that contributed to the reconstruction of a SARS-CoV-2 trimer looking model was used for the subsequent heterogeneous refinement of four models with the same *ab initio* volume. These four reconstructions revealed three different states, and the heterogeneous refinement was then repeated with three models. The resulting three particle stacks and three volumes were separately refined using homogeneous and non-uniform refinements in cryoSPARC. After rounds of refinement, the first particle stack with 178,597 particles yielded a reconstruction of 3.2 Å resolution with C3 symmetry. The second particle stack with 62,090 particles yielded a reconstruction of 3.7 Å resolution with C1 symmetry. And the last particle stack with 75,973 particles were discarded since the reconstruction had preferred orientation problem and it was similar to the first reconstruction. To resolve the residues at the interface of SARS-CoV-2 S 6P RBD and R40-1G8, a mask was generated using Chimera (Pettersen et al., 2004), and used for local refinement in cryoSPARC, which resulted in a final map of 3.5 Å local resolution using symmetry expanded (C3) particles. As the density for the RBD-Fab of the second reconstruction was bad, model buildings and structural refinements were only done for the first reconstruction. The initial model of SARS-CoV-2 S trimer in complex with R40-1G8 was obtained using the SARS-CoV-2 S 6P trimer (PDB 7K8T) and the C002 Fab structure (PDB 7K8O) as starting models. Initial model fitting was done in Chimera and Coot (Emsley et al., 2010). Rounds of refinements and manual model buildings were separately carried out in Phenix (Liebschner et al., 2020) and Coot, with final structure validation in Phenix.

QUANTIFICATION AND STATISTICAL ANALYSIS

Statistical modeling of SARS-CoV-2 sequences for identification of variants

The phylogeny was reconstructed using isolates of human SARS-CoV-2 retrieved from the GISAID EpiCov database (Elbe and Buckland-Merrett, 2017) as of 21-07-2021. Sequences that contained more than 1% ambiguous sites, with incomplete collection date or that diverged with more than 0.1 mutations per day from the root date, were removed, leaving more than 700.000 unique sequences. The sequences were aligned with MAFFTv7.467 (Katoh and Standley, 2013) to a reference isolate from GenBank (Wuhan-Hu-1, collected December 19th 2019 in Wuhan, China). This alignment of the selected isolates was used to infer the maximum likelihood phylogeny under the nucleotide substitution model GTR+G in IQTree (Minh et al., 2020). The tree topology was assessed using the ultrafast bootstrap function with 1000 replicates (Hoang et al., 2018). To root the tree, we specified the reference isolate hCoV-19/Wuhan/Hu-1/2019 (GISAID-Accession: EPI ISL 402125), which is identical in sequence to the GenBank isolate used in the alignment step. The sequences, as well as timing, of internal nodes were inferred using TreeTime. A fixed clock rate of 8×10^4 ($stdev = 46 \times 10^4$) (mutations / (bp date) was used under a skyline coalescent tree prior. The tree was rooted using the same reference isolate as with the IQTree step of topology reconstruction. The clock rate was computed as the total number of mutations on the tree, divided by the total length of branches of the timed tree. This rate was optimized by iterative runs of TreeTime (Sagulenko et al., 2018) until convergence. The maximum-likelihood time of the root of the tree is December 23, 2019.

Frequencies are computed as follows: (1) individual isolates, index with *i,* are assigned a smoothened multiplicity factor, $N_i(t) = \exp[-(t-t_i)^4/2\sigma^4] \times A_R(t)$, where t_i is the collection date of the isolate, and the squared Gaussian kernel is σ = 11 days. The regional epidemic factor $A_R(t)$ is the number of COVID-19 cases that are reported for each collected sequence on the tree in a region R: the multiplicity factor of an isolate reflects the likely number of SARS-CoV-2 cases in a given region R. Sample frequencies of the isolates are computed as $x_i(t) = N_i(t) / N(t)$, where $N(t) = \sum_i N_i(t)$. Global frequencies of particular clades or RBD mutants are then $X_\alpha(t) = \sum_{i \in \alpha} x_i(t)$, where the regional epidemic factor up- or downweighs regions that are under- or over-represented in the sequencing data. By construction of frequency trajectories $X_\alpha(t)$, the growth/decline of mutants can be tracked over time indicating mutations that might increase viral fitness.

Statistical analysis

Neutralizing levels of IgG (IC_{50}) or serum (ID_{50}) were calculated in GraphPad Prism 7.0 by using a non-linear fit model to plot an agonist versus normalized dose response curve with variable slope using the least-squares fitting method. A Y-value of 50% was used to calculate the corresponding X-value or IC_{50} based on this dose response curve. The statistical tests reported throughout the study were performed using GraphPad Prism 9.0. Data was checked for normality and the appropriate statistical test was applied. Significance was defined by considering P values < 0.05 as significant. The test applied for the individual analyses and P values are reported in the corresponding figure or figure legend. No additional methods were used to determine whether the data met assumptions of the statistical approach. Central tendencies are indicated in the corresponding figure or figure legend as median or geometric mean and denoted with bars. n values are defined in the corresponding figure legend to represent number of individuals, number of B cells or number of antibodies analyzed.

Cell Host & Microbe, Volume *30*

Supplemental information

Discovery of ultrapotent broadly neutralizing antibodies from SARS-CoV-2 elite neutralizers

Kanika Vanshylla, Chengcheng Fan, Marie Wunsch, Nareshkumar Poopalasingam, Matthijs Meijers, Christoph Kreer, Franziska Kleipass, Denis Ruchnewitz, Meryem S. Ercanoglu, Henning Gruell, Friederike Münn, Kai Pohl, Hanna Janicki, Tobias Nolden, Simone Bartl, Saskia C. Stein, Max Augustin, Felix Dewald, Lutz Gieselmann, Philipp Schommers, Thomas F. Schulz, Leif Erik Sander, Manuel Koch, Marta Łuksza, Michael Lässig, Pamela J. Bjorkman, and Florian Klein

Figure S1

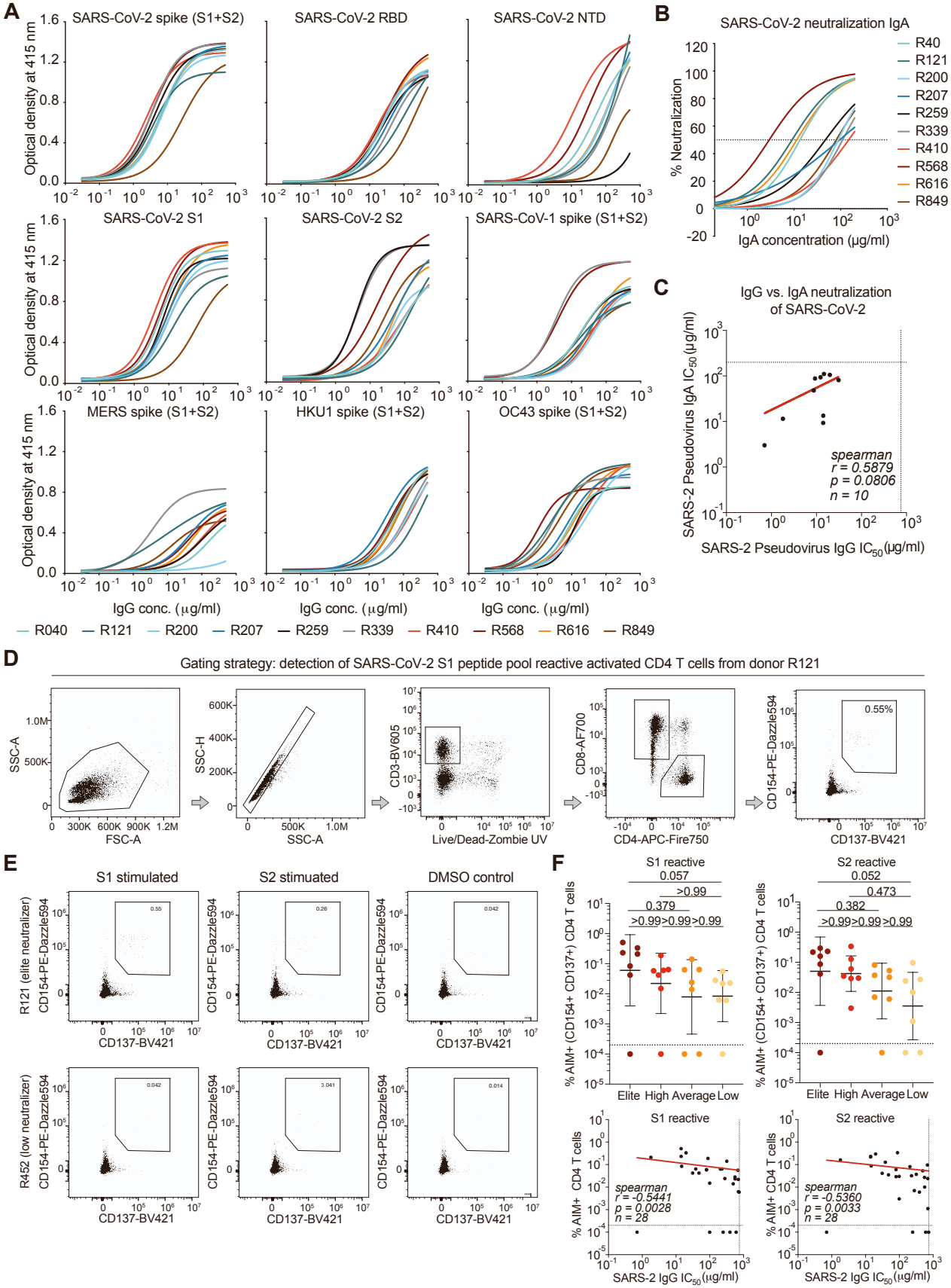

Figure S1: Coronavirus reactivity of elite neutralizers, related to Figure 1

A, ELISA-based binding curves depicting reactivity of elite neutralizer plasma IgG to SARS-CoV-2 spike trimer, RBD, NTD, S1, S2 as well as SARS-CoV-1 trimer, MERS trimer, HKU-1 spike and OC43 spike proteins. **B,** Neutralization curves depicting IgA neutralization from n=10 donor elite neutralizers against SARS-CoV-2 pseudovirus. Mean of two measurements plotted and dotted line represents 50% neutralization. **C,** Correlation plot between plasma purified IgG and IgA against SARS-CoV2 pseudovirus for 10 analyzed elite neutralizers. Dotted line represent limit of detection of assays; 750 μg/ml for IgG and 200 μg/ml for IgA. **D,** Gating strategy for detection of SARS-CoV-2 peptide pool reactive activated CD4 T cells as measured by presence of CD137+/CD154+ activation induced marker (AIM+) CD4 T cells. **E,** Exemplary plots of AIM+ expression on CD4+ T cells (of one elite- and one low-neutralizer after stimulation with S1 and S2 peptide pools as well as unstimulated control (DMSO). **F,** upper panel,T cell reactivity against SARS-CoV-2 S1 and S2 peptide pools in elite-, high-, average- and low-neutralizers (n=7 per group) as measured by activation induced marker (AIM+) CD137+/CD154+ CD4 T cells. Bars show geometric mean with 95%CI and statistical testing was done using the Kruskal-Wallis test. Values plotted below the dotted line did not show any detectable reactivity; lower panel, correlation plots between reactive AIM+ CD4 T cells and SARS-CoV-2 pseudovirus neutralization. Dotted lines denote limit of detection (IC_{50}) or values below dotted line did not show detectable reactivity (%AIM+ CD4 T cells).

Figure S2

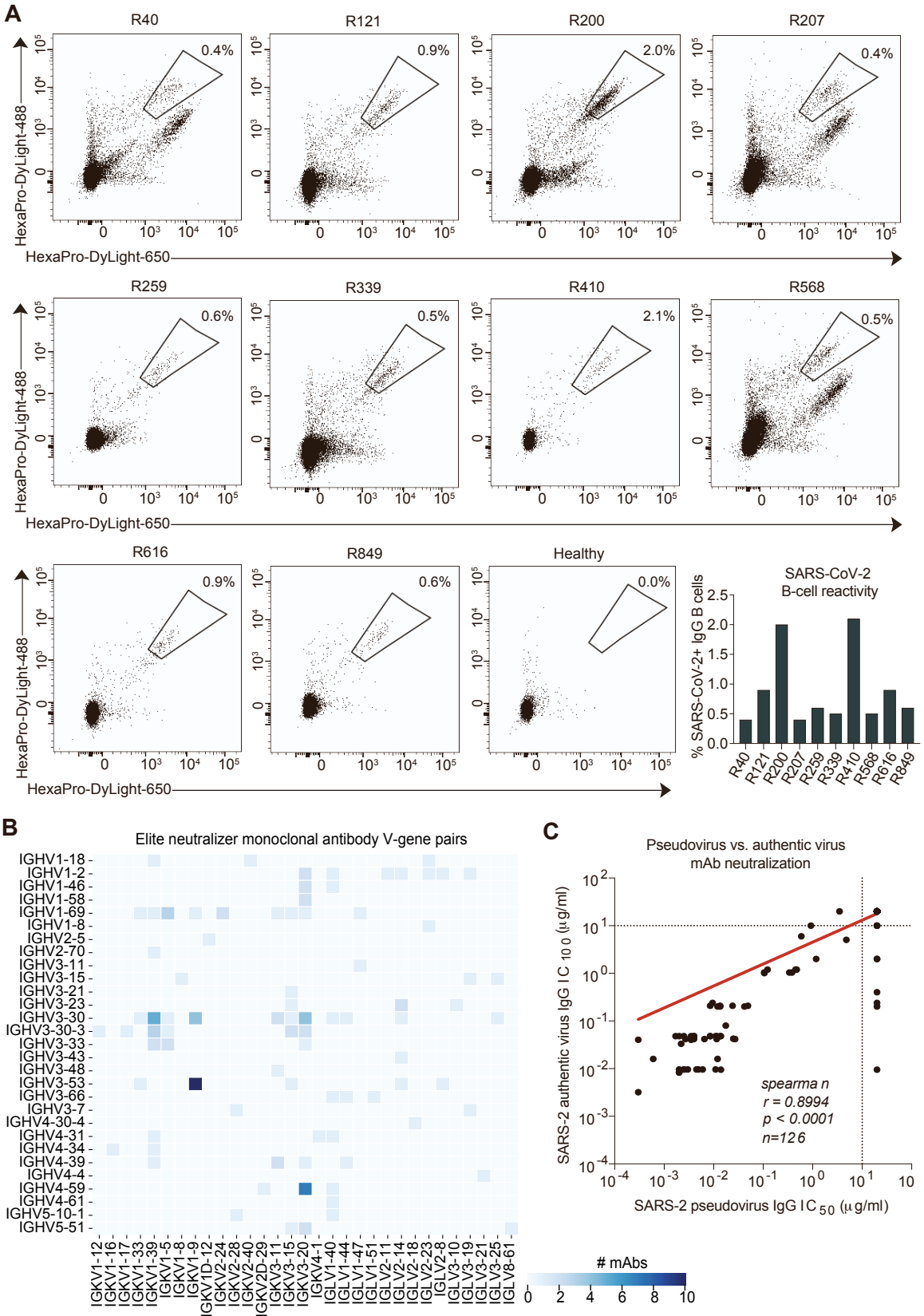

Figure S2: Fraction of SARS-CoV-2 reactive B cells from elite neutralizers and features of isolated mAbs, related to Figures 2 and 3

A, FACS plots and graph (lower right) showing the SARS-CoV-2 spike-reactive fraction amongst IgG+ B cells in elite neutralizers. **B,** Heat map illustrating the frequency of heavy and light V-gene combinations of the n=126 elite neutralizer derived mAbs produced and studied in detail. **C,** Correlation plot between SARS-CoV2 pseudovirus and authentic virus neutralization for n=126 tested mAbs. Dotted lines represent limit of detection of assays of 10 μg/ml IgG.

Figure S3

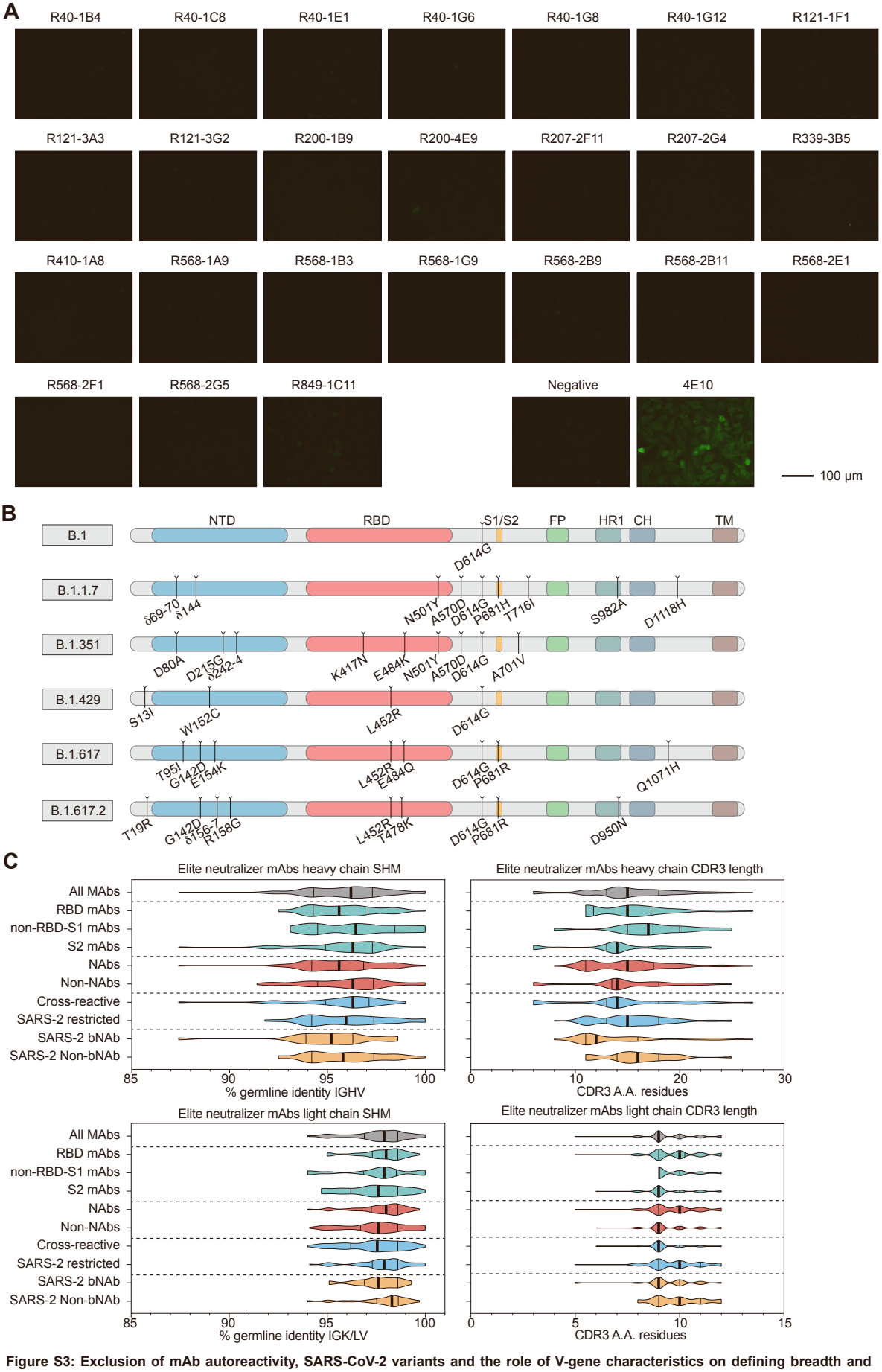

Figure S3: Exclusion of mAb autoreactivity, SARS-CoV-2 variants and the role of V-gene characteristics on defining breadth and potency of isolated NAbs, related to Figures 3 and 4

A, HEp-2 cell assay to screen for autoreactivity of selected mAbs tested at 100 µg/ml. **B,** Schematic of the SARS-COV-2 spike domains highlighting the residues mutated in the VOCs or VOIs used in the study. **C,** Analysis of the role of heavy chain (top panel) and light chain (lower panel) V-gene somatic hypermutation rate (left) and CDR3 length (left) in influencing spike binding patterns or SARS-CoV-2 pseudovirus neutralization potency of the mAbs (n=126).

Figure S4

* Emerging escape variants identified and functionally tested in this study. Note that D614G is designated B.1 based on pangolin lineage.

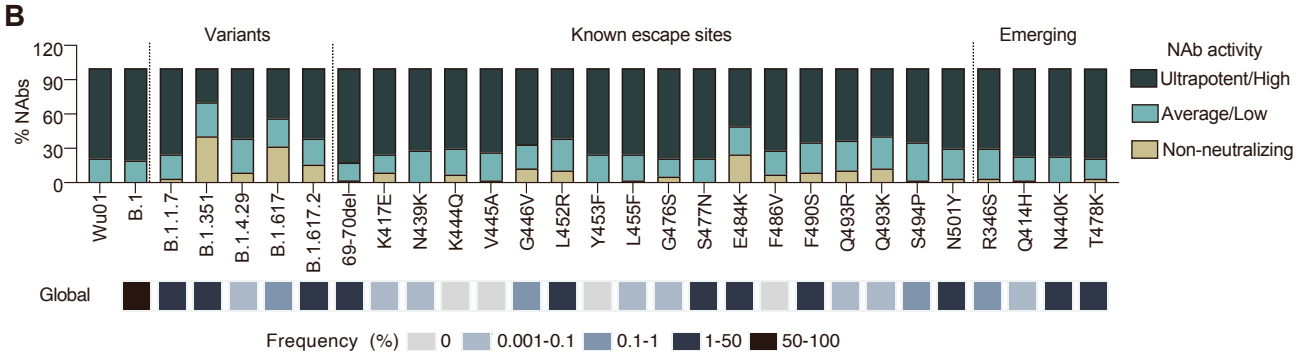

Figure S4: Frequency of known and emerging escape variants and potency of NAbs against them, related to Figure 5
A, Plots show the frequency distribution of the variants and escape sites from sequences downloaded on July 21st 2021. Frequencies are corrected for the collection date and total case counts in the region (see Methods). Countries with high vaccination rates (>60%) include UK and Israel. Countries and regions with low vaccination rates (<30%) include South America, Japan, India, Russia, Indonesia, Thailand, Iran Bangladesh, Vietnam, Africa. B, Plot depicting fraction of isolated NAbs which show ultrapotent/high neutralization (IC_{50} < 0.2 μg/ml, olive green), average/low neutralization (IC_{50} 0.2-10 μg/ml, light green) or complete escape (IC_{50}>10 μg/ml, golden) against the corresponding pseudovirus variant tested along with the respective global frequencies of respective variants (panel below).

Figure S5

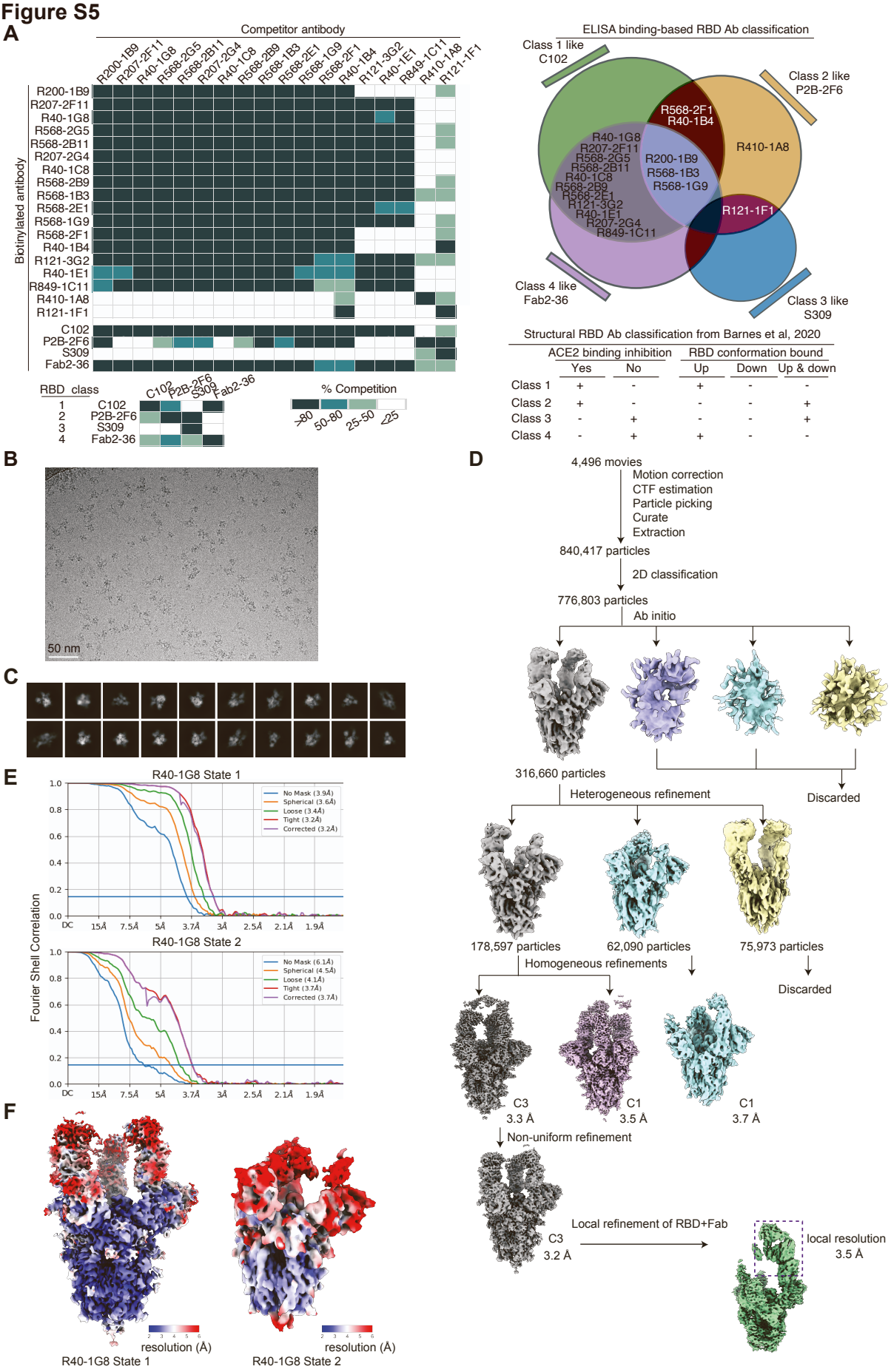

Figure S5: RBD class-mapping of bNAbs and CryoEM data processing and validation of R40-1G8 in complex with SARS-CoV-2 S protein, related to Figure 6.

A, Competition ELISA-based RBD epitope mapping of 18 RBD bNAbs with 100% breadth along with 1 mAb each from the 4 known RBD-binding epitope classes based on structural mapping. **B,** Representative micrograph (scale bar, 50 nm) **C,** 2D classes **D,** workflow of single-particle data processing **E,** Fourier shell correlation (FSC) plots and **F,** local resolution estimations for R40-1G8 in complex with SARS-CoV2-S. Two states of R40-1G8-SARS-CoV2-S complex were resolved, with one state having all 'up' RBDs, and the second state having 1 'up' RBD with R40-1G8 bound, 1 'down' RBD with R40-1G8 bound and 1 flexible 'up' RBD with no antibody binding.

Figure S6

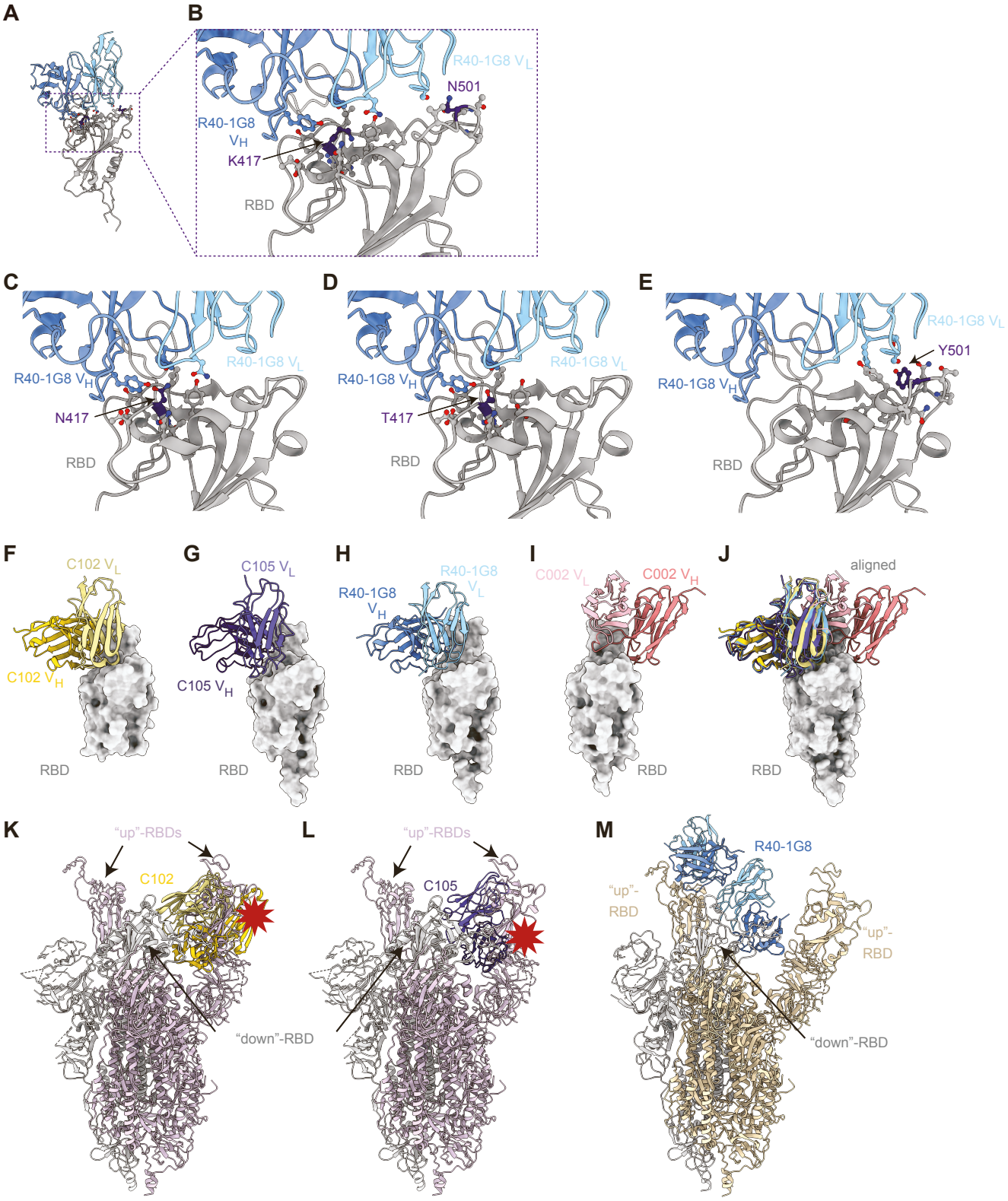

Figure S6: Predicted interactions of R40-1G8 Fab with two RBD residues that vary in SARS-CoV-2 VOC and structural comparisons of RBD class 1 antibodies, related to figure 6.
A, VH-VL domains of R40-1G8 Fab complexed with RBD. RBD positions K417 and 501 are highlighted in purple with sidechains in ball and stick representation. **B**, Close-up of R40-1G8 interactions with RBD residues near positions 417 and 501, the sites that are substituted in K417N/T and N501Y variants. Close-up views of R40-1G8 interactions with homology models of SARS-CoV-2 RBD including K417N (**C**), K417T (**D**), and N501Y (**E**) substitutions. Homology models were constructed using SWISS-Model, based on a high-resolution crystal structure of SARS-CoV-2 RBD (PDB 7EAM). Models of R40-1G8 Fab in complex with the RBD models were obtained by aligning the RBD portion of the R40-1G8 Fab-SARS-CoV-2 S 6P cryo-EM structure with the RBD homology models. Residues within 5 Å of RBD positions 417 and 501 are shown in ball and stick representation. **F-H**, Structures of the VH-VL domains of class 1 antibodies C102 (**F**) (PDB 7K8M), C105 (**G**) (PDB 6XCM), and R40-1G8 (**H**) (PDB 7SC1), demonstrating similar epitopes and binding poses. **I**, Structure of the VH-VL domains of the class 2 antibody C002 (PDB 7K8T) in complex with SARS-CoV-2 RBDs, demonstrating binding to a different RBD epitope. **J**, Overlay of C102, C105, R40-1G8 and C002 VH-VL domains bound to the SARS-CoV-2 RBD. **K-M**, Structural alignments on a 'down' RBD of an S trimer of the VH-VL domains for C102 (**K**) (PDB 7K8M) and C105 (**L**) (PDB 6XCM) showing that these Fabs would clash with a neighboring 'up' RBD, whereas the VH-VL domains of R40-1G8 (**M**) bound to a down RBD do not clash with neighboring 'up' RBDs.

Table S1: Demographics and the antibody response in study participants, related to Figure 1

A

Study ID	Age (years)	Gender	COVID-19 severity	Disease symptoms*	Pre-existing conditions**
R40	55	Male	Mild disease	1,2,3,5,6,7,8	None reported
R121	45	Male	Mild disease	1,2	None reported
R200	32	Female	Mild disease	1,4,7,8,9	None reported
R207	50	Female	Mild disease	1,2,3,4,5,6,7,8,9	None reported
R259	54	Female	Mild disease	2,8,9	None reported
R339	57	Male	Hospitalized	1,2,4,5,8,9	Heart attack
R410	55	Male	Mild disease	2,5,6,8,9	None reported
R568	60	Female	Hospitalized	1,3,5,7,8	Hypertension
R616	41	Male	Mild disease	1,5,6,8,9	Thrombocytopenia
R849	47	Female	Mild disease	1,2,3,4,6,8,9	Asthma

* 1 = Fever, 2= Cough, 3= Sore throat, 4= Rhinitis, 5= Muscle and body ache, 6= Headache, 7= Diarrhea, 8= Change in taste , 9 = Change in olfaction
** Conditions that are risk factors for COVID-19

B

Study ID	Weeks since disease onset	Neutralization IC_{50} (μg/ml)			ELISA Area under curve | EC50 in μg/ml															
		IgG SARS-2	IgG SARS-1	IgA SARS-2	SARS-2 Trimer		SARS-2 RBD		SARS-2 NTD		SARS-2 S1		SARS-2 S2		SARS-1 Trimer		MERS Trimer		HKU1 Trimer		OC43 Trimer	
R40	4.1	14.2	22.4	13.4	576	6.4	437	24.8	427	53.8	576	6.0	309	78.2	360	19.8	113	154.5	350	65.5	363	8.0
R121	4.6	14.1	47.9	9.3	478	3.7	344	125.4	403	103.1	425	13.3	311	151.9	291	16.3	255	8.4	193	403.9	463	2.9
R200	6.4	9.3	391.7	87.8	546	6.6	436	21.6	386	126.9	510	9.9	340	40.2	303	44.7	0	>500	260	147.5	384	29.2
R207	5.0	12.3	55.0	93.6	585	7.1	411	35.6	396	166.5	539	8.8	422	58.0	325	28.8	226	44.1	391	32.8	408	8.0
R259	5.4	8.7	61.8	48.0	585	4.3	405	23.4	38	>500	539	6.9	599	4.2	350	18.6	149	104.5	344	48.9	349	11.9
R339	6.1	14.7	40.4	110.5	615	3.6	382	43.1	331	204.9	474	8.8	595	4.5	517	3.5	357	3.6	280	161.1	417	2.7
R410	6.1	19.8	33.7	105.5	577	2.5	433	16.4	568	12.1	618	4.0	313	84.2	317	40.0	160	109.7	257	241.0	420	22.4
R568	8.6	0.7	12.1	3.0	618	3.6	487	29.1	533	32.0	615	5.8	587	17.1	511	4.0	202	44.4	353	41.9	359	1.1
R616	7.7	1.8	33.1	11.5	577	6.6	473	31.0	385	115.6	583	10.0	406	46.7	362	43.3	202	58.4	345	70.3	429	14.0
R849	9.6	31.0	5.1	80.9	450	27.0	263	235.5	178	156.3	326	64.4	455	26.0	279	25.1	184	13.3	339	69.2	454	4.4

C

Study ID	Age (years)	Gender	Disease severity	Neutralization group	IgG IC50 (mg/ml) SARS-2
R102	54	Male	Mild symptoms	High	99.3
R301	56	Fem	Mild symptoms	High	99.2
R501	45	Male	Mild symptoms	High	80.0
R561	44	Male	Mild symptoms	High	38.4
R702	43	Fem	Hospitalized	High	79.7
R759	52	Male	Mild symptoms	High	47.9
R851	53	Male	Mild symptoms	High	88.3
R10	54	Male	Asymptomatic	Average	206.0
R649	56	Fem	Mild symptoms	Average	318.8
R674	50	Fem	Mild symptoms	Average	248.1
R675	32	Male	Mild symptoms	Average	278.9
R679	47	Male	Mild symptoms	Average	229.2
R709	47	Male	Mild symptoms	Average	394.4
R803	29	Male	Mild symptoms	Average	493.0
R369	31	Fem	Mild symptoms	Low	703.9
R452	39	Male	Mild symptoms	Low	555.6
R456	36	Male	Mild symptoms	Low	696.8
R457	25	Fem	Mild symptoms	Low	679.4
R680	54	Fem	Mild symptoms	Low	740.0
R753	59	Fem	Mild symptoms	Low	562.8
R807	45	Male	Mild symptoms	Low	601.9

* T cell response compared to elite neutralizers R40, R121, R339, R410, R568, R616, R849

Table S2: Features of IGHV3-53 NAbs from SARS-CoV-2 elite neutralizers, related to Figure 4

Antibody	IGHV	CDRH3 a.a. length	CDRH3 Sequence	% Breadth	K417E escape	E484K escape	IGKV	Average** IC_{50} (µg/ml)
R207-2F11	IGHV3-53	11	ARDLVYRGMDV	100	No	No	IGKV1-33	0.0043
R40-1G8	IGHV3-53	11	ARDLYVFGMDV	100	No	No	IGKV1-9	0.0047
R568-2G5	IGHV3-53	11	ARDLYYYGMDV	100	No	No	IGKV1-9	0.0055
R568-2B11	IGHV3-53	11	TRDLVYYGMDV	100	No	No	IGKV1-9	0.0072
R207-2G4	IGHV3-53	11	ARDLVAYGMDV	100	No	No	IGKV1-9	0.0078
R40-1C8	IGHV3-53	11	VRDLVDYGMDV	100	No	No	IGKV1-9	0.0097
R568-2B9	IGHV3-53	11	ARDLVHYGMDV	100	No	No	IGKV1-9	0.0102
R568-1B3	IGHV3-53	11	ARDLVAYGMDV	100	No	No	IGKV1-9	0.0115
R568-2E1	IGHV3-53	11	ARDLIVYGMDV	100	No	No	IGKV1-9	0.0200
R207-2A6	IGHV3-53	11	ARDYGDYYFDY	96	Yes	No	IGKV3-15	0.0329
R207-2C2	IGHV3-53	12	ARGEGWDLPFDY	91	Yes	No	IGLV2-8	0.0096
R207-1C4	IGHV3-53	11	ARDRYVLGMDV	91	Partial*	No	IGKV1-9	1.1306
R568-1E8	IGHV3-53	11	ARDLDYYGMDV	83	Yes	No	IGKV1-9	0.1571
R616-1G4	IGHV3-53	15	ARDKRIPYYFYGMDV	70	No	Partial*	IGLV2-14	1.0849
C102	IGHV3-53	11	ARDYGDYYFDY	91	Yes	No	IGKV3-20	0.1146

* Partial escape when fold change in IC_{50} of greater than 10-fold observed
** Average IC_{50} based on neutralization profile against variants tested in Figure 4

Table S3: Cryo-EM data collection, refinement and validation statistics, related to Figure 6

	SARS-CoV-2 S 6P + R40-1G8 Fab
Data Collection and processing	
Microscope	Titan Krios at Caltech
Camera	Gatan K3
Magnification	x105,000
Voltage (keV)	300
Exposure (e/Å^2)	60
Pixel size (Å)	0.832
Defocus Range (μm)	- 1.0 to -3.0
Initial Particle Image (no.)	841,017
Final Particle Image (no.)	178,957
Symmetry Imposed	C3
Map Resolution (Å)	3.17
FSC Threshold	0.143
Map Resolution Range (Å)	3.1 - 3.4
Refinement	
Initial Model Used	PDB ID: 7K8T
Model Resolution (Å)	3.40
FSC Threshold	0.143
Model composition	
non-hydrogen atoms	29,415
protein residues	3,705
ligands	45
Average B-factors (Å^2)	
protein	142
ligands	135
R.m.s. deviations	
Bond length (Å)	0.006
Bond angles (°)	0.604
Validation	
MolProbity score	1.79
Clashscore	10.0
Rotamer outliers	0.06
Ramachandran plot	
Ramachandran favored (%)	96.02
Ramachandran allowed (%)	3.98
Ramachandran outliers (%)	0
PDB ID	7SC1